

Spectroscopic footprints of quantum friction in nonreciprocal and chiral media

O. J. Franca,^{1,*} Fabian Spallek,¹ Steffen Giesen,² Robert Berger,²
Kilian Singer,¹ Stefan Aull,¹ and Stefan Yoshi Buhmann^{1,†}

¹*Institut für Physik, Universität Kassel, Heinrich-Plett-Straße 40, 34132 Kassel, Germany*

²*Fachbereich Chemie, Philipps-Universität Marburg, Hans-Meerwein-Str 4, Marburg 35032, Germany*

We investigate how the quantum friction experienced by a polarizable atom moving with constant velocity parallel to a planar interface is modified when the latter consists of chiral or nonreciprocal media, with special focus on topological insulators. We use macroscopic quantum electrodynamics to obtain the velocity-dependent Casimir–Polder frequency shift and decay rate. These results are a generalization to matter with time-reversal symmetry breaking. We illustrate our findings by examining the nonretarded and retarded limits for five examples: a perfectly conducting mirror, a perfectly reflecting nonreciprocal mirror, a three-dimensional topological insulator, a perfectly reflecting chiral mirror and an isotropic chiral medium. We find different asymptotic power laws for all these materials. Interestingly, we find two bridges between chirality and nonreciprocity through the frequency shift that arise as a consequence of the magnetoelectric coupling. Namely, the position-dependent Casimir–Polder frequency shift for the nonreciprocal case depend on a geometric magnetic field associated with photoionization of chiral molecules, the Casimir–Polder depending on the velocities for the chiral case have the optical rotatory strength as the atomic response while those for the nonreciprocal case depend on an analog of the optical rotatory strength.

I. INTRODUCTION

The research in quantum friction is deeply connected with observable macroscopic effects produced by quantum vacuum fluctuations of the electromagnetic field, of which the attractive Casimir force between two neutral bodies [1–4] and the Casimir-Polder force between an atom and a neutral body [5] are the most renowned. When two uncharged polarizable bodies move relative to each other at constant velocity, a dissipative force that works against the relative motion is experienced on each of them due to the exchange of Doppler-shifted virtual photons at zero temperature. This effect is what we know as quantum friction [6–10]. Assuming that the surfaces of the moving bodies are flat and perfectly smooth, quantum friction could be understood as a van der Waals type attraction originated from electric dipoles created by the quantum fluctuations in one of the surfaces and the induced image electric dipoles on the other surface, which lag behind when the bodies are in relative parallel motion [6]. Quantum friction has also been predicted to arise in particle-surface (Casimir-Polder) interactions [11–14], where the velocity and distance dependency of the drag force in three-dimensional bulk materials is analysed. In this regard, studies in graphene have been carried out recently [15].

Quantum friction has a quantum origin and the physics behind it is related to the quantum Cherenkov effect through the anomalous Doppler effect [16–19], where real photons are extracted from the vacuum at the cost of the object’s kinetic energy; they are absorbed and emitted, thus producing a fluctuating momentum recoil [20].

Considering only an atomic translational motion, spin-zero photons are absorbed and reemitted which translates in an overall quantum frictional force that opposes the translational motion. In recent years, this process has been investigated in several scenarios [21–24] and its outstanding connection to nonequilibrium physics was recently figured out [25]. This idea plus allowing for atomic rotational degrees of freedom, results in what is called quantum rolling friction [26]. Note that the related phenomenon of Coulomb drag [27], in which a current in one plate induces a voltage bias in another via the fluctuating Coulomb field, has been successfully demonstrated [28].

In order to gain further insights into quantum friction, a different path has been taken in the works [9, 24]. Particularly, in the article [24] by using the framework of macroscopic QED [29–31] the authors are able to provide testable quantities with direct experimental contrast in the context of the Casimir-Polder force leading to the prediction of a velocity-dependent quantum-vacuum effect. Concretely, this work reports atomic level shifts and rates of spontaneous decay for a zero-temperature neutral atom with dipole moment and nonrelativistic velocity moving next to a perfectly smooth macroscopic surface, which in principle can be measured. Also important efforts have recently been done to obtain a satisfactory description of quantum friction in all timescales regarding carefully all the typical approximations for this phenomenon such as Markovianity, linear response theory, for example [32].

Besides the fundamental research of quantum friction, it has also been studied in innovative setups such as the flow of water in carbon nanochannels, where quantum friction is the dominant friction mechanism for water on carbon-based materials [33]. This phenomenon has been investigated in new kinds of materials such as bidimensional topological materials [10]. For instance, exposing quantum friction to a two-dimensional topological mate-

*Electronic address: uk081688@uni-kassel.de

†Electronic address: stefan.buhmann@uni-kassel.de

rial enables an increase of two orders of magnitude in the quantum drag force with respect to conventional neutral graphene systems [10]. So, the jump to three-dimensional topological insulators (TIs) will open the gate to the interplay between quantum friction generated by an atom with constant velocity and the topological magnetoelectric effect provided by the TI, to which this paper is devoted.

Three-dimensional TIs are a novel state of matter exhibiting insulating bulk and conducting surface states protected by time-reversal symmetry [34, 35]. The articles [36, 37] predicted their topological behavior where two types have been distinguished: strong three-dimensional TIs exhibit an odd number of surface states on each surface, whereas the weak ones have an even number of them on all but a single surface [36, 38]. Then, $\text{Bi}_{1-x}\text{Sb}_x$ was confirmed as the first strong three-dimensional TI in the work [39]. This paved the way to detect a huge variety of TIs as reported in [40] and the more recently discovered new class of topological insulators, called axion insulators [41]. They have the same bulk as TIs, with gapped bulk and surface states, where the topological properties are protected by inversion, instead of time reversal symmetry. They can arise up in magnetically doped-TI heterostructures with magnetization pointing inwards and outwards from the top and bottom interfaces of the TI [41]. When the interface between a 3D strong TI and a regular insulator presents time-reversal symmetry breaking, either by the application of a magnetic coating and/or by doping the TI with transition metal elements, the opening of the gap in the surface states induces several exotic phenomena which can be tested experimentally. Among them we find the quantum anomalous Hall effect [42, 43], the quantized magneto-optical effect [44, 45], the topological magnetoelectric effect [34, 46, 47] and even radiative effects [48–51]. Also the image magnetic monopole effect has been analyzed in [52] but its direct experimental verification still remains an open challenge. Combinations of TIs with other kind of systems with interesting electromagnetic responses such as semiconductor quantum dots has been already analyzed in [53] showing that the applications and research on TIs are promissory and almost endless. These effects can be also produced in axion insulators.

Another scenario where quantum friction has been investigated is in presence of chiral media as Ref. [54], to which this paper is devoted as well. A three-dimensional object that cannot be superimposed on its mirror image is said to be chiral, these distinct mirror images are called enantiomers. Spectroscopically, enantiomers have identical transition energies and distinguishing between the two is not trivial. The characteristic feature of chiral objects is the manner of their interactions with other chiral objects. For example, the refractive indices of left- and right-handed circularly polarized light are different in a chiral medium, therefore the two polarizations will propagate at different speeds. The difference in velocity

is related to the phenomenon of optical activity. Circular dichroism is closely related where the wave with the ‘slower’ polarization is absorbed more strongly as it travels through the medium [55].

Many of the processes crucial to life involve chiral molecules whose chiral identity plays a central role in their chemical reactions. The undesired enantiomer can react differently, thereby not producing the required result. In nature, these chiral molecules predominantly, or even exclusively, occur in one enantiomeric form, so that their reactions proceed differently when different enantiomers are present. In contrast, artificial production without addition of enriched enantiomers or other chiral agents creates both enantiomers in equal proportions. Therefore it is important to be able to distinguish between enantiomers and ultimately to be able to separate a racemic (containing both enantiomers) mixture into an enantiomerically pure sample.

A frequently used method to separate enantiomers in an industrial setting is enantioselective chromatography. The initial racemic solution is passed through a column packed with a resolving agent, which by necessity has to be chiral. This either retards, or stops, the progress of one of the enantiomers passing through the column but crucially not for the other and thus allows the solution to be separated. From an optical viewpoint it has been proposed that a racemic sample can be purified by use of coordinated laser pulses, which use a two-step process to initially drive different transitions in the enantiomers before converting one into the other [56]. It has recently been calculated that in the presence of a chiral carbon nanotube the enantiomers of alanine possess different absorption energies and it was theorized that this could lead to a method of discrimination [57]. Furthermore, it has been shown that the van der Waals dispersion force between molecules can be enantiomer selective [58, 59]. In fact, there have been a lot of efforts to provide a selection and distinguishing method such as the use of the Casimir-Polder force [60–62]. For all these reasons, we will also explore how the quantum friction is modified in these materials.

Due to the fact that TIs break time-reversal symmetry, they can be regarded as nonreciprocal media [63, 64]. In this way, the theory of macroscopic QED cannot be directly applied because it is based on Lorentz’s reciprocity principle (a particular case of the Onsager reciprocity from statistical physics [65]) stating the reversibility of optical paths. In terms of symmetry, it is equivalent to invariance under an exchange of positions and orientations of sources and fields. Thus media respecting this principle are called reciprocal and preserve time-reversal symmetry. To deal with nonreciprocal media, which violate Lorentz’s principle relation [66], macroscopic QED was generalized to include the necessary features of nonreciprocal media in Ref. [63]. The aim of the present paper is to study the Casimir-Polder frequency shift and decay rate on a parallel moving atom to a nonreciprocal medium. This paper is organized as follows: in Section

II we calculate the time-dependent electric and magnetic field in the framework of macroscopic QED for nonreciprocal media. This result is obtained through a direct quantization of the noise current. Section III is devoted to study how the internal atomic dynamics is modified by the nonreciprocal media. To this end, we present modified equations for the frequency shift and decay rate that depend on the atom position as well as on its velocity. In Section IV we apply our results to a polarizable charged particle moving with constant velocity parallel to five different materials: a perfectly conducting mirror, a perfectly reflecting nonreciprocal mirror, a strong three-dimensional topological insulator, a perfectly reflecting chiral mirror and an isotropic chiral medium. In Section V we provide numerical results for the frequency shift with electrical dipole transition via Rydberg states and discuss the viability of an experimental verification. Section VI comprises a concluding summary of our results.

II. THE TIME-DEPENDENT ELECTROMAGNETIC FIELD

Due to time-reversal symmetry violation in nonreciprocal media, the Lorentz reciprocity principle for the Green's tensor [66] is no longer valid

$$\mathbb{G}(\mathbf{r}, \mathbf{r}'; \omega) \neq \mathbb{G}^\top(\mathbf{r}', \mathbf{r}; \omega) \quad (1)$$

where \top denotes the matrix transpose. This requires to introduce generalised definitions for the real and imaginary parts of the Green's tensor \mathbb{G}

$$\mathcal{R}[\mathbb{G}(\mathbf{r}, \mathbf{r}'; \omega)] = \frac{1}{2} [\mathbb{G}(\mathbf{r}, \mathbf{r}'; \omega) + \mathbb{G}^{*\top}(\mathbf{r}', \mathbf{r}; \omega)] , \quad (2)$$

$$\mathcal{I}[\mathbb{G}(\mathbf{r}, \mathbf{r}'; \omega)] = \frac{1}{2i} [\mathbb{G}(\mathbf{r}, \mathbf{r}'; \omega) - \mathbb{G}^{*\top}(\mathbf{r}', \mathbf{r}; \omega)] . \quad (3)$$

For a reciprocal medium with $\mathbb{G}(\mathbf{r}, \mathbf{r}'; \omega) = \mathbb{G}^\top(\mathbf{r}', \mathbf{r}; \omega)$, they reduce to ordinary, component-wise real and imaginary parts. The general expressions for the field operators in frequency space read

$$\begin{aligned} \hat{\mathbf{E}}(\mathbf{r}) &= \int_0^\infty d\omega \left[\hat{\mathbf{E}}(\mathbf{r}; \omega) + \hat{\mathbf{E}}^\dagger(\mathbf{r}; \omega) \right] , \\ \hat{\mathbf{B}}(\mathbf{r}) &= \int_0^\infty d\omega \left[\hat{\mathbf{B}}(\mathbf{r}; \omega) + \hat{\mathbf{B}}^\dagger(\mathbf{r}; \omega) \right] . \end{aligned} \quad (4)$$

where \dagger denotes hermitian conjugation in operator space which is distinct from \top^* , i.e. complex conjugation and matrix transpose in three-dimensional position space. The electric field can be computed through the Green's tensor in the following way

$$\begin{aligned} \hat{\mathbf{E}}(\mathbf{r}; \omega) &= i\mu_0\omega \left[\mathbb{G} \star \hat{\mathbf{j}}_N \right] (\mathbf{r}; \omega) , \\ &= i\mu_0\omega \int d^3r' \mathbb{G}(\mathbf{r}, \mathbf{r}'; \omega) \cdot \hat{\mathbf{j}}_N(\mathbf{r}'; \omega) , \end{aligned} \quad (5)$$

where \star denotes spatial convolution and $\hat{\mathbf{j}}_N$ is the noise current density governed by the quantum fluctuations

occurring in the medium and with a vanishing average $\langle \hat{\mathbf{j}}_N \rangle = \mathbf{0}$. The corresponding expression for the magnetic field $\hat{\mathbf{B}}$ is obtained by using the Faraday's law in the frequency space

$$\hat{\mathbf{B}}(\mathbf{r}; \omega) = \mu_0 \int d^3r' \nabla \times \mathbb{G}(\mathbf{r}, \mathbf{r}'; \omega) \cdot \hat{\mathbf{j}}_N(\mathbf{r}'; \omega) . \quad (6)$$

In order to obtain the time-dependent electric field, we must find a solution for the time-dependent creation $\hat{\mathbf{f}}^\dagger$ and annihilation $\hat{\mathbf{f}}$ operators. To this end, we will directly quantize the noise current density $\hat{\mathbf{j}}_N$ following the noise-current-based schema, as we shall expose in Sec. II A. The Hamiltonian \hat{H} for the atom-field system is composed of the atomic part \hat{H}_A , the field part \hat{H}_F , and a contribution for the atom-field interaction \hat{H}_{AF} , meaning that $\hat{H} = \hat{H}_A + \hat{H}_{AF} + \hat{H}_F$. The atomic part is given by

$$\hat{H}_A = \sum_n E_n \hat{A}_{nn} , \quad (7)$$

which incorporates the eigenenergies E_n for each atomic energy level and the atomic flip operators $\hat{A}_{mn} = |m\rangle\langle n|$. The Hamiltonian \hat{H}_F comprises the integral over all the frequency-dependent number operators of the field-medium system

$$\hat{H}_F = \int d^3\mathbf{r} \int_0^\infty d\omega \hbar\omega \hat{\mathbf{f}}^\dagger(\mathbf{r}; \omega) \cdot \hat{\mathbf{f}}(\mathbf{r}; \omega) , \quad (8)$$

which clearly resembles a quantum harmonic oscillator and can be cast through the quantization of the noise current; cf. Sec. II A. The interaction Hamiltonian \hat{H}_{AF} for nonmagnetic atoms in multipolar coupling and long wavelength approximation couples the atomic dipole to the electromagnetic field as

$$\begin{aligned} \hat{H}_{AF} &= -\hat{\mathbf{d}} \cdot \hat{\mathbf{E}}(\mathbf{r}_A) + \dot{\mathbf{r}}_A \cdot \hat{\mathbf{d}} \times \hat{\mathbf{B}}(\mathbf{r}_A) , \\ &= -\sum_{m,n} \hat{A}_{mn} \left[\mathbf{d}_{mn} \cdot \hat{\mathbf{E}}(\mathbf{r}_A) + \mathbf{v} \cdot \mathbf{d}_{mn} \times \hat{\mathbf{B}}(\mathbf{r}_A) \right] , \end{aligned} \quad (9)$$

and contains the electric-dipole operator $\hat{\mathbf{d}} = \sum_{m,n} \mathbf{d}_{mn} \hat{A}_{mn}$, \mathbf{r}_A is the position of the atom and $\dot{\mathbf{r}}_A = \mathbf{v}$ its velocity. As the atomic Hamiltonian \hat{H}_A and the field operators commute, only the resulting commutation relations for these operators with the field Hamiltonian \hat{H}_F and the interaction Hamiltonian \hat{H}_{AF} deserve to be studied to find the expression for the electric field (4).

A. Electromagnetic field in terms of noise currents

In this subsection, we proceed to solve the equations of motion of the field operators. For this aim, the noise

current is quantized directly by expressions for the field operators. In frequency space, Ohm's law reads

$$\hat{\mathbf{j}}(\mathbf{r}; \omega) = \left[\mathbb{Q} \star \hat{\mathbf{E}} \right] (\mathbf{r}; \omega) + \hat{\mathbf{j}}_N(\mathbf{r}; \omega), \quad (10)$$

which describes the response of a linear medium with conductivity matrix \mathbb{Q} to the electric field $\hat{\mathbf{E}}(\mathbf{r}; \omega)$. Thereby, we write down the Helmholtz equations as follows

$$\left[\nabla \times \nabla - \frac{\omega^2}{c^2} \right] \mathbb{G}(\mathbf{r}, \mathbf{r}'; \omega) - i\mu_0 \omega [\mathbb{Q} \star \mathbb{G}] (\mathbf{r}, \mathbf{r}'; \omega) = \delta(\mathbf{r} - \mathbf{r}') \mathbb{I}. \quad (11)$$

One finds the formal solution for this equation by employing the boundary condition $\mathbb{G}(\mathbf{r}, \mathbf{r}'; \omega) \rightarrow \mathbb{O}$ for $\|\mathbf{r} - \mathbf{r}'\| \rightarrow \infty$, which leads to Eq. (5).

Next, we quantize the noise-current density $\hat{\mathbf{j}}_N$ introduced in Eq. (5) simply by writing it in terms of creation $\hat{\mathbf{f}}^\dagger$ and annihilation $\hat{\mathbf{f}}$ operators

$$\hat{\mathbf{j}}_N(\mathbf{r}; \omega) = \sqrt{\frac{\hbar \omega}{\pi}} \left[\mathbb{R} \star \hat{\mathbf{f}} \right] (\mathbf{r}; \omega), \quad (12)$$

where \mathbb{R} is a square root of the positive definite conductivity tensor and is related to it by [63]

$$\left[\mathbb{R} \star \mathbb{R}^{*\top} \right] (\mathbf{r}, \mathbf{r}'; \omega) = \mathcal{R} [\mathbb{Q}(\mathbf{r}, \mathbf{r}'; \omega)]. \quad (13)$$

With all the above, we obtain the Heisenberg equation of motion for the annihilation operator $\hat{\mathbf{f}}$ as shown

$$\dot{\hat{\mathbf{f}}}(\mathbf{r}; \omega) = \frac{1}{i\hbar} \left[\hat{\mathbf{f}}(\mathbf{r}; \omega), \hat{H} \right], \quad (14)$$

where the three summands of \hat{H} are given by Eqs. (7), (8) and (9). Nevertheless, it proves convenient to rewrite the interaction Hamiltonian \hat{H}_{AF} in terms of field operators,

$$\begin{aligned} \hat{H}_{AF} &= -i\mu_0 \sum_{m,n} \int_0^\infty \omega d\omega \sqrt{\frac{\hbar \omega}{\pi}} \hat{A}_{mn} \\ &\times \mathbf{d}_{mn} \cdot \left\{ \left[\mathbb{G} \star \mathbb{R} \star \hat{\mathbf{f}} \right] (\mathbf{r}_A; \omega) - \left[\mathbb{G}^* \star \mathbb{R}^* \star \hat{\mathbf{f}}^\dagger \right] (\mathbf{r}_A; \omega) \right\} \\ &+ \mu_0 \sum_{m,n} \int_0^\infty \frac{d\omega}{i\omega} \sqrt{\frac{\hbar \omega}{\pi}} \hat{A}_{mn} \\ &\times \mathbf{v} \cdot \mathbf{d}_{mn} \times \left\{ \nabla \times \left[\mathbb{G} \star \mathbb{R} \star \hat{\mathbf{f}} \right] (\mathbf{r}_A; \omega) \right. \\ &\left. - \nabla \times \left[\mathbb{G}^* \star \mathbb{R}^* \star \hat{\mathbf{f}}^\dagger \right] (\mathbf{r}_A; \omega) \right\}. \quad (15) \end{aligned}$$

In this way, the solution for the annihilation operator $\hat{\mathbf{f}}$ is given by

$$\begin{aligned} \hat{\mathbf{f}}(\mathbf{r}; \omega, t) &= e^{-i\omega(t-t_0)} \hat{\mathbf{f}}(\mathbf{r}; \omega) + \frac{\mu_0 \omega}{\hbar} \sqrt{\frac{\hbar \omega}{\pi}} \sum_{m,n} \int_{t_0}^t dt' \\ &\times \left\{ e^{-i\omega(t-t')} \left[\mathbb{G} \star \mathbb{R} \right]^{*\top} (\mathbf{r}_A(t'), \mathbf{r}; \omega) \cdot \mathbf{d}_{mn} \hat{A}_{mn}(t') \right. \\ &+ \frac{e^{-i\omega(t-t')}}{\omega^2} \left(\left[\mathbb{G} \star \mathbb{R} \right]^{*\top} (\mathbf{r}, \mathbf{r}_A(t'); \omega) \times \overleftarrow{\nabla} \right) \\ &\left. \times \mathbf{d}_{mn} \cdot \mathbf{v} \hat{A}_{mn}(t') \right\}, \quad (16) \end{aligned}$$

where one should notice that $\overleftarrow{\nabla}$ acts on the second argument of the Green's tensor. Also here we have required that $\hat{\mathbf{f}}(\mathbf{r}; \omega, t_0) = \hat{\mathbf{f}}(\mathbf{r}; \omega)$, i.e. the Heisenberg-picture operator agrees with its time-dependent Schrödinger-picture at initial time t_0 .

Assuming that the atom moves with nonrelativistic speed, $v \ll c$, will enforce us to seek a solution to the atom-field dynamics that is correct within leading linear order of v/c . According to the Born-Oppenheimer approximation, we may assume the center of mass velocity to remain constant on the time-scale relevant for the internal atom-field dynamics, so that [31]

$$\mathbf{r}_A(t') = \mathbf{r}_A(t) + (t-t')\mathbf{v}. \quad (17)$$

Once this approximation is substituted into the solution for the annihilation operator (16) and discarding quadratic terms in v/c , we find that

$$\begin{aligned} \hat{\mathbf{f}}(\mathbf{r}; \omega, t) &= e^{-i\omega(t-t_0)} \hat{\mathbf{f}}(\mathbf{r}; \omega) + \frac{\mu_0 \omega}{\hbar} \sqrt{\frac{\hbar \omega}{\pi}} \sum_{m,n} \int_{t_0}^t dt' \\ &\times \left\{ e^{-i\omega(t-t')} \left[\mathbb{G} \star \mathbb{R} \right]^{*\top} (\mathbf{r}_A(t), \mathbf{r}; \omega) \cdot \mathbf{d}_{mn} \hat{A}_{mn}(t') \right. \\ &- (t-t') e^{-i\omega(t-t')} \left[\mathbb{G} \star \mathbb{R} \right]^{*\top} (\mathbf{r}_A(t), \mathbf{r}; \omega) \\ &\cdot \mathbf{d}_{mn} (\overleftarrow{\nabla} \cdot \mathbf{v}) \hat{A}_{mn}(t') \\ &+ \frac{e^{-i\omega(t-t')}}{\omega^2} \left(\left[\mathbb{G} \star \mathbb{R} \right]^{*\top} (\mathbf{r}, \mathbf{r}_A(t); \omega) \times \overleftarrow{\nabla} \right) \\ &\left. \times \mathbf{d}_{mn} \cdot \mathbf{v} \hat{A}_{mn}(t') \right\}. \quad (18) \end{aligned}$$

After substituting the Eq. (18) into Eq. (12) and employing Eq. (13) and simplifying through the next integral relation for the Green's tensor in nonreciprocal media [63]

$$\mathcal{I} [\mathbb{G}(\mathbf{r}, \mathbf{r}'; \omega)] = \mu_0 \omega \left[\mathbb{G} \star \mathcal{R} [\mathbb{Q}] \star \mathbb{G}^{*\top} \right] (\mathbf{r}, \mathbf{r}'; \omega), \quad (19)$$

we finally obtain expressions for the electric

$$\begin{aligned} \hat{\mathbf{E}}(\mathbf{r}; \omega, t) &= e^{-i\omega(t-t_0)} \hat{\mathbf{E}}(\mathbf{r}; \omega) + \frac{i\mu_0 \omega^2}{\pi} \sum_{m,n} \int_{t_0}^t dt' \\ &\times \left\{ e^{-i\omega(t-t')} \mathcal{I} [\mathbb{G}(\mathbf{r}, \mathbf{r}_A(t); \omega)] \cdot \mathbf{d}_{mn} \hat{A}_{mn}(t') \right. \\ &- (t-t') e^{-i\omega(t-t')} \mathcal{I} [\mathbb{G}(\mathbf{r}, \mathbf{r}_A(t); \omega)] \\ &\cdot \mathbf{d}_{mn} (\overleftarrow{\nabla} \cdot \mathbf{v}) \hat{A}_{mn}(t') \\ &+ \frac{e^{-i\omega(t-t')}}{i\omega} \left(\mathcal{I} [\mathbb{G}(\mathbf{r}, \mathbf{r}_A(t); \omega)] \times \overleftarrow{\nabla} \right) \\ &\left. \times \mathbf{d}_{mn} \cdot \mathbf{v} \hat{A}_{mn}(t') \right\}, \quad (20) \end{aligned}$$

and magnetic fields

$$\begin{aligned} \hat{\mathbf{B}}(\mathbf{r}; \omega, t) &= e^{-i\omega(t-t_0)} \hat{\mathbf{B}}(\mathbf{r}; \omega) + \frac{\mu_0 \omega}{\pi} \sum_{m,n} \int_{t_0}^t dt' \\ &\times \left\{ e^{-i\omega(t-t')} \nabla \times \mathcal{I} [\mathbb{G}(\mathbf{r}, \mathbf{r}_A(t); \omega)] \cdot \mathbf{d}_{mn} \hat{A}_{mn}(t') \right\} \\ &+ \mathcal{O}(v), \quad (21) \end{aligned}$$

where we only considered the zero-order approximation in v/c because the magnetic field appears in conjunction with a factor \mathbf{v} . In the latter equation, we remark that ∇ acts only on the first argument of the Green's tensor.

Brief observations on Eqs. (20) and (21) should be given. First, Eq. (20) extends the result for an atom at rest in nonreciprocal media of the work [64] to a moving atom. Second, the Eq. (21) generalizes the standard magnetic field to the case of nonreciprocal media [29]. And both expressions differ from the usual expressions for reciprocal media only by the redefinition of the imaginary part of the Green's tensor defined in Eq. (3).

III. INTERNAL ATOMIC DYNAMICS: FREQUENCY SHIFT AND DECAY RATE

The internal atomic dynamics can be described by the Heisenberg equations of motion for the flip operator

$$\dot{\hat{A}}_{mn} = \frac{1}{i\hbar} [\hat{A}_{mn}, \hat{H}] = \frac{1}{i\hbar} [\hat{A}_{mn}, \hat{H}_A] + \frac{1}{i\hbar} [\hat{A}_{mn}, \hat{H}_{AF}], \quad (22)$$

which does not include the field Hamiltonian \hat{H}_F because it commutes with the flip operator. Our approach follows the procedure for a reciprocal surface fully detailed in Ref. [31] and the one applied for a nonreciprocal surface with an atom at rest of Ref. [64], now extended to a moving atom parallel to the surface.

This leads to

$$\begin{aligned} \dot{\hat{A}}_{mn} &= i\omega_{mn}\hat{A}_{mn} + \frac{i}{\hbar} \sum_k \int_0^\infty d\omega \\ &\times \left\{ \left(\hat{A}_{mk} \mathbf{d}_{nk} - \hat{A}_{kn} \mathbf{d}_{km} \right) \cdot \left[\hat{\mathbf{E}}(\mathbf{r}_A; \omega) + \mathbf{v} \times \hat{\mathbf{B}}(\mathbf{r}_A; \omega) \right] \right. \\ &\left. + \left[\hat{\mathbf{E}}^\dagger(\mathbf{r}_A; \omega) + \mathbf{v} \times \hat{\mathbf{B}}^\dagger(\mathbf{r}_A; \omega) \right] \cdot \left(\mathbf{d}_{nk} \hat{A}_{mk} - \mathbf{d}_{km} \hat{A}_{kn} \right) \right\}, \end{aligned}$$

which appears in normal ordering and does not show the time-dependence for brevity.

To evaluate the required time integrals we will make some approximations. Firstly, we will assume weak atom-field coupling, which will require that the field spectrum $\omega^2 \mathcal{I}[\mathbb{G}(\mathbf{r}_A(t), \mathbf{r}_A(t); \omega)]$ is sufficiently flat [31]. Particularly, it must not exhibit any narrow peaks in the vicinity of any atomic transition frequency. Secondly, we will assume that \hat{A}_{mn} is dominated by oscillations with frequencies $\tilde{\omega}_{mn}$ which are yet to be determined in a self-consistent manner. Lastly, we will formally carry out the time integrals by means of the Markov approximation. Thus, we are allowed to neglect the slow non-oscillatory dynamics of the atomic flip operator \hat{A}_{mn} during the time interval $t' \in [t_0, t]$, so we may set $\hat{A}_{mn}(t') \simeq \exp[i\tilde{\omega}_{mn}(t' - t)]\hat{A}_{mn}(t)$, where we foresee that the property $\tilde{\omega}_{mn} = -\tilde{\omega}_{nm}$ must be verified. Then,

we send $t_0 \rightarrow -\infty$ in the time integral obtaining

$$\begin{aligned} \hat{A}_{mn}(t) &\int_{t_0}^t dt' e^{-i(\omega - \tilde{\omega}_{nm})(t-t')} \\ &\simeq \hat{A}_{mn}(t) \int_{-\infty}^t dt' e^{-i(\omega - \tilde{\omega}_{nm})(t-t')}, \\ &= \hat{A}_{mn}(t) \left[\pi \delta(\omega - \tilde{\omega}_{nm}) - i \frac{\mathcal{P}}{\omega - \tilde{\omega}_{nm}} \right]. \quad (23) \end{aligned}$$

By taking the derivative with respect to ω of this result, we determine the remaining time integral

$$\begin{aligned} &\int_{t_0}^t dt' (t - t') e^{-i\omega(t-t')} \hat{A}_{mn}(t') \\ &\simeq \frac{d}{d\omega} \left[\frac{\mathcal{P}}{\omega - \tilde{\omega}_{nm}} + i\pi \delta(\omega - \tilde{\omega}_{nm}) \right] \hat{A}_{mn}(t). \quad (24) \end{aligned}$$

For both results \mathcal{P} stands for the Cauchy principle value and the limits of the frequency integral of Eq. (27) will lead to the appearance of Heaviside function ϑ .

By defining the coefficient

$$\mathbf{C}_{mn} = \mathbf{C}_{mn}(\mathbf{r}_A) + \mathbf{C}_{mn}(\mathbf{r}_A, \mathbf{v}), \quad (25)$$

which contains a pure position-dependent component [64]

$$\begin{aligned} \mathbf{C}_{mn}(\mathbf{r}_A) &= \frac{\mu_0}{\hbar} \vartheta(\tilde{\omega}_{mn}) \tilde{\omega}_{mn}^2 \mathcal{I}[\mathbb{G}(\mathbf{r}_A, \mathbf{r}_A; \tilde{\omega}_{mn})] \cdot \mathbf{d}_{mn} \\ &\quad - \frac{i\mu_0}{\pi\hbar} \mathcal{P} \int_0^\infty \frac{\omega^2 d\omega}{\omega - \tilde{\omega}_{nk}} \mathcal{I}[\mathbb{G}(\mathbf{r}_A, \mathbf{r}_A; \omega)] \cdot \mathbf{d}_{mn}, \quad (26) \end{aligned}$$

as well as a position- and velocity-dependent one

$$\begin{aligned} \mathbf{C}_{mn}(\mathbf{r}_A, \mathbf{v}) &= \\ &\frac{i\mu_0}{\hbar} \vartheta(\tilde{\omega}_{mn}) \left\{ \omega^2 \mathcal{I}[\mathbb{G}(\mathbf{r}_A, \mathbf{r}_A; \omega)] \right\}'_{\omega=\tilde{\omega}_{nm}} \cdot \mathbf{d}_{mn} (\hat{\nabla} \cdot \mathbf{v}) \\ &+ \frac{\mu_0}{\pi\hbar} \mathcal{P} \int_0^\infty \frac{d\omega}{\omega - \tilde{\omega}_{nm}} \left\{ \omega^2 \mathcal{I}[\mathbb{G}(\mathbf{r}_A, \mathbf{r}_A; \omega)] \right\}' \cdot \mathbf{d}_{mn} (\hat{\nabla} \cdot \mathbf{v}) \\ &- \frac{i\mu_0}{\hbar} \vartheta(\tilde{\omega}_{mn}) \tilde{\omega}_{nm} \left\{ \mathcal{I}[\mathbb{G}(\mathbf{r}_A, \mathbf{r}_A; \tilde{\omega}_{nm})] \times \hat{\nabla} \right\} \times \mathbf{d}_{mn} \cdot \mathbf{v} \\ &- \frac{\mu_0}{\pi\hbar} \mathcal{P} \int_0^\infty \frac{\omega d\omega}{\omega - \tilde{\omega}_{nm}} \left\{ \mathcal{I}[\mathbb{G}(\mathbf{r}_A, \mathbf{r}_A; \omega)] \times \hat{\nabla} \right\} \times \mathbf{d}_{mn} \cdot \mathbf{v} \\ &- \frac{i\mu_0}{\hbar} \vartheta(\tilde{\omega}_{mn}) \tilde{\omega}_{nm} \mathbf{v} \times \left\{ \nabla \times \mathcal{I}[\mathbb{G}(\mathbf{r}_A, \mathbf{r}_A; \tilde{\omega}_{nm})] \right\} \cdot \mathbf{d}_{mn} \\ &- \frac{\mu_0}{\pi\hbar} \mathcal{P} \int_0^\infty \frac{\omega d\omega}{\omega - \tilde{\omega}_{nm}} \mathbf{v} \times \left\{ \nabla \times \mathcal{I}[\mathbb{G}(\mathbf{r}_A, \mathbf{r}_A; \omega)] \right\} \cdot \mathbf{d}_{mn}, \end{aligned}$$

where primes in the first and second term denote derivatives with respect to the respective frequency arguments.

We are able to cast Eq. (23) into the form

$$\begin{aligned}
\hat{A}_{mn}(t) &= i\omega_{mn}\hat{A}_{mn}(t) + \frac{i}{\hbar} \sum_k \int_0^\infty d\omega \\
&\times \left\{ e^{-i\omega(t-t_0)} \left[\hat{A}_{mk}(t)\mathbf{d}_{nk} - \hat{A}_{kn}(t)\mathbf{d}_{km} \right] \right. \\
&\cdot \left[\hat{\mathbf{E}}(\mathbf{r}_A; \omega) + \mathbf{v} \times \hat{\mathbf{B}}(\mathbf{r}_A; \omega) \right] \\
&+ e^{i\omega(t-t_0)} \left[\hat{\mathbf{E}}^\dagger(\mathbf{r}_A; \omega) + \mathbf{v} \times \hat{\mathbf{B}}^\dagger(\mathbf{r}_A; \omega) \right] \\
&\cdot \left(\mathbf{d}_{nk}\hat{A}_{mk}(t) - \mathbf{d}_{km}\hat{A}_{kn}(t) \right) \\
&- \sum_{k,l} \left[\mathbf{d}_{nk} \cdot \mathbf{C}_{kl}\hat{A}_{ml}(t) - \mathbf{d}_{km} \cdot \mathbf{C}_{nl}\hat{A}_{kl}(t) \right] \\
&+ \sum_{k,l} \left[\mathbf{d}_{nk} \cdot \mathbf{C}_{ml}^*\hat{A}_{lk}(t) - \mathbf{d}_{km} \cdot \mathbf{C}_{kl}^*\hat{A}_{ln}(t) \right],
\end{aligned} \tag{27}$$

where we have used the identity $\mathcal{I}[\mathbb{G}^*(\mathbf{r}_A, \mathbf{r}_A; \omega)] = \mathcal{I}[\mathbb{G}^\dagger(\mathbf{r}_A, \mathbf{r}_A; \omega)]$, which is deduced from Eq. (3). The main difference between Eq. (27) and the one for the reciprocal case lies on the redefinition of the imaginary part of the Green's tensor introduced by the coefficients (26) and (27).

Next, we take expectation values of Eq. (27) assuming that the electromagnetic field is prepared in its ground state at initial time t_0 , which implies that $\hat{\mathbf{E}}(\mathbf{r}; \omega)|\{0\rangle\rangle = \mathbf{0}$, $\forall \mathbf{r}, \omega$. This also means that the involved density matrix reads $\hat{\rho}_0 = |\{0\rangle\rangle\langle\{0|\}$. As a consequence of normal ordering the free contributions of the electric and magnetic field will be zero.

Now, we need to solve Eq. (27). To this end, we assume the atom to be free of quasidegenerate transitions. Additionally, the atom is assumed to be unpolarized in each of its energy eigenstates, i.e. $\mathbf{d}_{nn} = \mathbf{0}$, as well as that its states of a degenerate manifold are not connected by electric-dipole transitions $\mathbf{d}_{nn'} = \mathbf{0}$. Both conditions are guaranteed by atomic selection rules [31]. Under these conditions, the fast-oscillating off-diagonal flip operators decouple from the nonoscillating diagonal ones as well as from each other [31].

For $m \neq n$, under the above assumptions, we obtain that

$$\begin{aligned}
\langle \hat{A}_{mn}(t) \rangle &= i\omega_{mn}\langle \hat{A}_{mn}(t) \rangle \\
&- \sum_k (\mathbf{d}_{nk} \cdot \mathbf{C}_{kn} + \mathbf{d}_{km} \cdot \mathbf{C}_{km}^*) \langle \hat{A}_{mn}(t) \rangle.
\end{aligned} \tag{28}$$

For $m = n$, the diagonal flip operators are non-oscillating and mutually coupled. After retaining only diagonal terms on Eq. (27), we find

$$\begin{aligned}
\langle \hat{A}_{nn}(t) \rangle &= - \sum_k (\mathbf{d}_{nk} \cdot \mathbf{C}_{kn} + \mathbf{d}_{kn} \cdot \mathbf{C}_{kn}^*) \langle \hat{A}_{nn}(t) \rangle \\
&+ \sum_k (\mathbf{d}_{kn} \cdot \mathbf{C}_{nk} + \mathbf{d}_{nk} \cdot \mathbf{C}_{nk}^*) \langle \hat{A}_{kk}(t) \rangle.
\end{aligned} \tag{29}$$

By virtue of Eq. (3) the two terms $\mathbf{d}_{nk} \cdot \mathcal{I}[\mathbb{G}(\mathbf{r}_A, \mathbf{r}_A; \omega)] \cdot \mathbf{d}_{kn} = \text{Im}[\mathbf{d}_{nk} \cdot \mathbb{G}(\mathbf{r}_A, \mathbf{r}_A; \omega) \cdot \mathbf{d}_{kn}]$ and $\mathbf{d}_{kn} \cdot \mathcal{I}[\mathbb{G}^\dagger(\mathbf{r}_A, \mathbf{r}_A; \omega)] \cdot \mathbf{d}_{nk} = \text{Im}[\mathbf{d}_{nk} \cdot \mathbb{G}(\mathbf{r}_A, \mathbf{r}_A; \omega) \cdot \mathbf{d}_{kn}]$ are equal and real. This will occur for the real parts too.

At this point is worth mentioning that the Green's tensor \mathbb{G} can be split into a bulk part $\mathbb{G}^{(0)}$ and a scattering part $\mathbb{G}^{(1)}$. Here we will assume that the Lamb shift associated with the free-space Green's tensor $\mathbb{G}^{(0)}$ is already included in the bare transition frequency ω_{mn} by making the replacement $\mathbb{G} \rightarrow \mathbb{G}^{(1)}$, which refers only to the atom and does not consider the material properties of surrounding matter [29]. Hence, the remaining frequency shift stems from the presence of electromagnetic bodies around the atom.

So, taking real and imaginary parts of the coefficients in Eqs. (28) and (29) according to

$$\sum_k \mathbf{d}_{nk} \cdot \mathbf{C}_{kn} = \frac{\Gamma_n}{2} + i\delta\omega_n, \tag{30}$$

$$\sum_k \mathbf{d}_{kn} \cdot \mathbf{C}_{kn}^* = \frac{\Gamma_n}{2} - i\delta\omega_n, \tag{31}$$

we are able to identify the decay rate

$$\begin{aligned}
\Gamma_n &= \Gamma_n(\mathbf{r}_A) + \Gamma_n(\mathbf{r}_A, \mathbf{v}), \\
&= \sum_k \Gamma_{nk} = \sum_{k < n} \Gamma_{nk}(\mathbf{r}_A) + \sum_k \Gamma_{nk}(\mathbf{r}_A, \mathbf{v}),
\end{aligned} \tag{32}$$

and the frequency shift

$$\begin{aligned}
\delta\omega_n &= \delta\omega_n(\mathbf{r}_A) + \delta\omega_n(\mathbf{r}_A, \mathbf{v}), \\
&= \sum_k \delta\omega_{nk} = \sum_k \delta\omega_{nk}(\mathbf{r}_A) + \sum_{k < n} \delta\omega_{nk}(\mathbf{r}_A, \mathbf{v}),
\end{aligned} \tag{33}$$

with the position-dependent contributions [64]

$$\Gamma_{nk}(\mathbf{r}_A) = \frac{2\mu_0}{\hbar} \tilde{\omega}_{nk}^2 \text{Im} \left[\mathbf{d}_{nk} \cdot \mathbb{G}^{(1)}(\mathbf{r}_A, \mathbf{r}_A; \tilde{\omega}_{nk}) \cdot \mathbf{d}_{kn} \right], \tag{34}$$

$$\begin{aligned}
\delta\omega_{nk}(\mathbf{r}_A) &= -\frac{\mu_0}{\pi\hbar} \mathcal{P} \int_0^\infty \frac{\omega^2 d\omega}{\omega - \tilde{\omega}_{nk}} \\
&\times \text{Im} \left[\mathbf{d}_{nk} \cdot \mathbb{G}^{(1)}(\mathbf{r}_A, \mathbf{r}_A; \omega) \cdot \mathbf{d}_{kn} \right],
\end{aligned} \tag{35}$$

and the position- and velocity-dependent contributions

$$\begin{aligned}
\Gamma_{nk}(\mathbf{r}_A, \mathbf{v}) &= \\
&\frac{2\mu_0}{\pi\hbar} \mathcal{P} \int_0^\infty \frac{d\omega}{\omega - \tilde{\omega}_{nk}} \\
&\times \left\{ \omega^2 \mathcal{I} \left[\mathbf{d}_{nk} \cdot (\mathbf{v} \cdot \nabla) \mathbb{G}^{(1)}(\mathbf{r}_A, \mathbf{r}_A; \omega) \cdot \mathbf{d}_{kn} \right] \right\}' \\
&- \frac{2\mu_0}{\pi\hbar} \mathcal{P} \int_0^\infty \frac{\omega d\omega}{\omega - \tilde{\omega}_{nk}} \\
&\times \mathbf{d}_{nk} \cdot \left\{ \mathcal{I} \left[\mathbb{G}^{(1)}(\mathbf{r}_A, \mathbf{r}_A; \omega) \right] \times \overleftarrow{\nabla} \right\} \times \mathbf{d}_{kn} \cdot \mathbf{v} \\
&- \frac{2\mu_0}{\pi\hbar} \mathcal{P} \int_0^\infty \frac{\omega d\omega}{\omega - \tilde{\omega}_{nk}} \\
&\times \mathbf{d}_{nk} \cdot \mathbf{v} \times \left\{ \nabla \times \mathcal{I} \left[\mathbb{G}^{(1)}(\mathbf{r}_A, \mathbf{r}_A; \omega) \right] \right\} \cdot \mathbf{d}_{kn},
\end{aligned} \tag{36}$$

$$\begin{aligned}
\delta\omega_{nk}(\mathbf{r}_A, \mathbf{v}) = & \\
& \frac{\mu_0}{2i\hbar} \left[\omega^2 \mathbf{d}_{kn} \cdot (\mathbf{v} \cdot \nabla') \mathbb{G}^{(1)\top}(\mathbf{r}, \mathbf{r}'; \omega) \cdot \mathbf{d}_{nk} \right]_{\substack{\omega=\tilde{\omega}_{nk} \\ \mathbf{r}=\mathbf{r}'=\mathbf{r}_A}}' \\
& - \frac{\mu_0}{2i\hbar} \left[\omega^2 \mathbf{d}_{nk} \cdot (\mathbf{v} \cdot \nabla') \mathbb{G}^{(1)\top*}(\mathbf{r}, \mathbf{r}'; \omega) \cdot \mathbf{d}_{kn} \right]_{\substack{\omega=\tilde{\omega}_{nk} \\ \mathbf{r}=\mathbf{r}'=\mathbf{r}_A}}' \\
& - \frac{\mu_0}{\hbar} \tilde{\omega}_{nk} \\
& \times \text{Im} \left\{ \mathbf{v} \cdot \mathbf{d}_{kn} \times \left[\nabla \times \mathbb{G}^{(1)\top}(\mathbf{r}', \mathbf{r}; \tilde{\omega}_{nk}) \right] \cdot \mathbf{d}_{nk} \right\}_{\mathbf{r}=\mathbf{r}'=\mathbf{r}_A} \\
& + \frac{\mu_0}{\hbar} \tilde{\omega}_{nk} \\
& \times \text{Im} \left\{ \mathbf{v} \cdot \mathbf{d}_{nk} \times \left[\nabla \times \mathbb{G}^{(1)}(\mathbf{r}, \mathbf{r}'; \tilde{\omega}_{nk}) \right] \cdot \mathbf{d}_{kn} \right\}_{\mathbf{r}=\mathbf{r}'=\mathbf{r}_A} .
\end{aligned} \tag{37}$$

From Eqs. (36) and (37) we observe that the second and third terms can be traced back to the last four terms of the coefficient $\mathbf{C}_{mn}(\mathbf{r}_A, \mathbf{v})$ defined in Eq. (27). In fact, for an atom with time-reversal invariant internal Hamiltonian and hence real dipole-matrix elements, such terms will cancel pairwise and will not contribute. However, in the present work we will take into account all these terms of $\mathbf{C}_{mn}(\mathbf{r}_A, \mathbf{v})$, because we will choose dipole moments such that the atom is sensitive to chiral media or the violated time-symmetry of the nonreciprocal media. Our choice is based on Curie's principle, which states that a system consisting of a crystal and an external influence, each having a specific symmetry, only maintains the symmetries that are shared by both the crystal and the external influence [69].

With the definitions (36) and (37), the equations of motion (28) and (29) for the expectation values of the atomic flip operators take the final form

$$\langle \dot{\hat{A}}_{mn}(t) \rangle = \left[i\tilde{\omega}_{mn} - \frac{1}{2}(\Gamma_m + \Gamma_n) \right] \langle \hat{A}_{mn}(t) \rangle, \tag{38}$$

$$\langle \dot{\hat{A}}_{nn}(t) \rangle = -\Gamma_n \langle \hat{A}_{nn}(t) \rangle + \sum_{k < n} \Gamma_{nk} \langle \hat{A}_{kk}(t) \rangle, \tag{39}$$

where we have identified the frequencies

$$\tilde{\omega}_{mn} = \omega_{mn} + \delta\omega_m - \delta\omega_n, \tag{40}$$

which verifies the property $\tilde{\omega}_{mn} = -\tilde{\omega}_{nm}$ previously mentioned. The appearance of the shifted frequency $\tilde{\omega}_{nk}$ in the expression for $\delta\omega_{nk}$ through the contributions $\delta\omega_{nk}(\mathbf{r}_A)$ (35) and $\delta\omega_{nk}(\mathbf{r}_A, \mathbf{v})$ (37) itself, the frequency shift is given as a self-consistent result from the implicit equation.

Henceforth we restrict our analysis only on the frequency shifts (35) and (37), which can be further simplified by using the redefinition of the imaginary part of the Green's tensor (3), the Schwarz principle valid for nonreciprocal media too,

$$\mathbb{G}^*(\mathbf{r}_A, \mathbf{r}_A; \omega) = \mathbb{G}^*(\mathbf{r}_A, \mathbf{r}_A; -\omega^*), \tag{41}$$

and the substitution $\omega \rightarrow -\omega$ in their second integrals arising from Eq. (3). The integral contours

along the positive and negative axes have one pole each and are evaluated in the ω -complex plane. The path along the quarter circle does not contribute because $\lim_{|\omega| \rightarrow 0} \omega^2 \mathbb{G}^{(1)}(\mathbf{r}_A, \mathbf{r}_A; \omega)/c^2 = \mathbb{O}$. The part along the imaginary axis leads to the position-dependent non-resonant frequency shift [64]

$$\begin{aligned}
\delta\omega_{nk}^{\text{res}}(\mathbf{r}_A) = & \frac{\mu_0}{\pi\hbar} \int_0^\infty \frac{\xi^3 d\xi}{\xi^2 + \tilde{\omega}_{nk}^2} \\
& \times \text{Im} \left[\mathbf{d}_{nk} \cdot \mathbb{G}^{(1)}(\mathbf{r}_A, \mathbf{r}_A; i\xi) \cdot \mathbf{d}_{kn} \right] \\
& - \frac{\mu_0}{\pi\hbar} \int_0^\infty \frac{\xi^2 \tilde{\omega}_{nk} d\xi}{\xi^2 + \tilde{\omega}_{nk}^2} \\
& \times \text{Re} \left[\mathbf{d}_{nk} \cdot \mathbb{G}^{(1)}(\mathbf{r}_A, \mathbf{r}_A; i\xi) \cdot \mathbf{d}_{kn} \right], \tag{42}
\end{aligned}$$

with a Green's function $\mathbb{G}^{(1)}$ with imaginary frequency $\omega \rightarrow i\xi$.

The evaluation of the poles gives the resonant contribution associated with the real-photon emission and a real-frequency expression $\tilde{\omega}_{nk}$ [64]

$$\delta\omega_{nk}^{\text{res}}(\mathbf{r}_A) = -\frac{\mu_0}{\hbar} \tilde{\omega}_{nk}^2 \text{Re} \left[\mathbf{d}_{nk} \cdot \mathbb{G}^{(1)}(\mathbf{r}_A, \mathbf{r}_A; \tilde{\omega}_{nk}) \cdot \mathbf{d}_{kn} \right]. \tag{43}$$

From Eq. (42) we observe that the matrix-vector product of the Green's tensor and the dipole moments is real for a reciprocal medium and therefore only the second contribution remains in this case [64]. Additionally, in Eq. (37) we appreciate another requirement for a non-zero contribution, which is that the Green's tensor of the corresponding material must have a curl different from zero. Remarkably, this last condition is satisfied for certain reciprocal media opening the gate to probe quantum friction in chiral materials for example. The case of chiral media will be analyzed in detail in the next section.

IV. APPLICATIONS

Once we have derived expressions for the frequency shift Eqs. (37), (42) and (43), we proceed to apply our findings for three ideal media: a perfectly conducting mirror, a perfectly reflecting nonreciprocal mirror, and a perfectly reflecting chiral mirror. Afterward, as more realistic examples, we illustrate our results for a strong three-dimensional TI and an isotropic chiral medium. In this work, we consider the configuration depicted in Fig. 1, where we consider a bi-layer configuration with the vacuum as upper layer and the nonreciprocal medium or the chiral medium as the lower layer. For this selection of five media, we restrict ourselves to real and constant permittivity, permeability and cross-susceptibility unless the contrary is specified.

The scattering part of the Green's tensor $\mathbb{G}^{(1)}$ of a

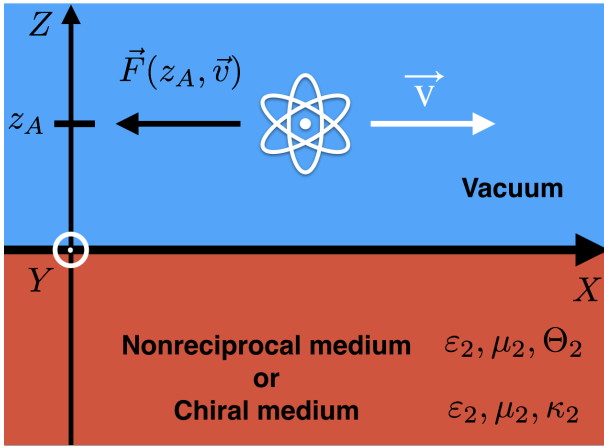


FIG. 1: Quantum friction experienced by an atom moving with constant velocity parallel to a planar interface made of vacuum and a nonreciprocal medium or of vacuum and a chiral medium. The experienced force is $\mathbf{F}(z_A, \mathbf{v})$ but is not treated in this work. Instead we study the frequency shift and decay rate induced in the atom.

single planar surface has the form [70]

$$\mathbb{G}^{(1)}(\mathbf{r}, \mathbf{r}'; \omega) = \frac{i}{8\pi^2} \int \frac{d^2 \mathbf{k}_{\parallel}}{k_{\perp}} \sum_{\sigma=s,p} \sum_{\sigma'=s,p} r_{\sigma, \sigma'} \times \mathbf{e}_{\sigma+} \otimes \mathbf{e}_{\sigma'-} e^{i\mathbf{k}_{\parallel} \cdot (\mathbf{r} - \mathbf{r}')} e^{ik_{\perp}(z+z')}, \quad (44)$$

where $\mathbf{e}_{\sigma+}$ and $\mathbf{e}_{\sigma'-}$ are the polarization unit vectors for σ - and σ' -polarized waves in the upper layer of Fig. 1. The indices s and p refer to perpendicular or parallel polarization, respectively. Here \mathbf{k}_{\parallel} represents the parallel component of the wave vector, k_{\perp} stands for its perpendicular component, and z denotes the vertical distance to the interface.

As mentioned in Section III, based on Curie's principle [69], to probe how the atom is sensitive to the violated time-reversal symmetry of a nonreciprocal medium or parity of a chiral medium, we must select dipole moments that share the same violated symmetry. To be as general as possible, we choose the following dipole moments

$$\mathbf{d}_{nk} = (d_{nk}^x, d_{nk}^y, d_{nk}^z)^{\top}, \quad \mathbf{d}_{kn} = \mathbf{d}_{nk}^*. \quad (45)$$

where $d_{nk}^x, d_{nk}^y, d_{nk}^z \in \mathbb{C}$ implying that such dipoles are not invariant if the direction of time is reversed $t \rightarrow -t$ as long as two of their components are not null. Actually, if $d_{nk}^x = d_{nk}/\sqrt{2}$, $d_{nk}^y = id_{nk}/\sqrt{2}$ and $d_{nk}^z = 0$ give circularly polarized dipoles which were employed in the article [64] and their fields propagate along the z direction. Additionally, due to our interest in quantum friction closer to the interface between the materials, we will take the velocity of the atom with $v_z = \mathbf{v} \cdot \mathbf{e}_z = 0$, meaning that all the velocity-dependent quantities will depend only on $\mathbf{v}_{\parallel} = v_x \mathbf{e}_x + v_y \mathbf{e}_y$. Also we have to consider another constriction for the dipole moments and

the velocity $\mathbf{v}_{\parallel} \cdot \mathbf{d}_{nk} = 0$, which is imposed by Maxwell equations.

A. Perfectly conducting mirror

The reflective coefficients for a perfectly conducting mirror are $r_{p,p} = 1$, $r_{s,s} = -1$ and $r_{p,s} = r_{s,p} = 0$. This set of coefficients is obtained from the reflective coefficients for a general material in the limit $\epsilon \rightarrow \infty$, which is explained in detail in Ref. [64]. For this mirror the Green's tensor (44) is only diagonal with

$$\mathbb{G}_{xx}^{(1)}(\mathbf{r}, \mathbf{r}; \omega) = \left(-\frac{1}{8\pi z} - \frac{ic}{16\pi\omega z^2} + \frac{c^2}{32\pi\omega^2 z^3} \right) e^{\frac{2i\omega z}{c}}, \quad (46)$$

$$\mathbb{G}_{yy}^{(1)}(\mathbf{r}, \mathbf{r}; \omega) = \mathbb{G}_{xx}^{(1)}(\mathbf{r}, \mathbf{r}; \omega), \quad (47)$$

$$\mathbb{G}_{zz}^{(1)}(\mathbf{r}, \mathbf{r}; \omega) = \left(-\frac{ic}{8\pi\omega z^2} + \frac{c^2}{16\pi\omega^2 z^3} \right) e^{\frac{2i\omega z}{c}}. \quad (48)$$

The contributions to the frequency shift (33) for the dipole (45) in the retarded limit ($\tilde{\omega}_{nk} z_A/c \gg 1$) read as follows

$$\delta\omega_{nk}^{\text{res,ret}}(\mathbf{r}_A) = \frac{\mu_0 \tilde{\omega}_{nk}^2}{8\pi\hbar} \left[\frac{|\mathbf{d}_{nk}^{\parallel}|^2}{z_A} \cos\left(\frac{2\tilde{\omega}_{nk} z_A}{c}\right) - \frac{c|d_{nk}^z|^2}{\tilde{\omega}_{nk} z_A^2} \sin\left(\frac{2\tilde{\omega}_{nk} z_A}{c}\right) \right], \quad (49)$$

$$\delta\omega_{nk}^{\text{nres,ret}}(\mathbf{r}_A) = \frac{c|\mathbf{d}_{nk}^{\parallel}|^2}{32\pi^2 \hbar \epsilon_0 \tilde{\omega}_{nk} z_A^4}, \quad (50)$$

$$\begin{aligned} \delta\omega_{nk}^{\text{ret}}(\mathbf{r}_A, \mathbf{v}) &= \frac{\mu_0 \tilde{\omega}_{nk}^2 S_{nk}(\mathbf{v}_{\parallel})}{4\pi\hbar c z_A} \sin\left(\frac{2\tilde{\omega}_{nk} z_A}{c}\right) \\ &= 0, \end{aligned} \quad (51)$$

where $\mathbf{d}_{nk}^{\parallel} = d_{nk}^x \mathbf{e}_x + d_{nk}^y \mathbf{e}_y$ and z_A is the distance of the atom to the interface. For the nonretarded limit ($\tilde{\omega}_{nk} z_A/c \ll 1$), we find

$$\delta\omega_{nk}^{\text{res,nret}}(\mathbf{r}_A) = -\frac{1}{16\pi\hbar\epsilon_0 z_A^3} \left[\frac{1}{2} |\mathbf{d}_{nk}^{\parallel}|^2 + |d_{nk}^z|^2 \right], \quad (52)$$

$$\delta\omega_{nk}^{\text{nres,nret}}(\mathbf{r}_A) = \frac{1}{32\pi^2 \hbar \epsilon_0 z_A^3} \left[\frac{1}{2} |\mathbf{d}_{nk}^{\parallel}|^2 + |d_{nk}^z|^2 \right], \quad (53)$$

$$\delta\omega_{nk}^{\text{nret}}(\mathbf{r}_A, \mathbf{v}) = \frac{\mu_0 \tilde{\omega}_{nk} S_{nk}(\mathbf{v}_{\parallel})}{8\pi\hbar z_A^2} = 0. \quad (54)$$

We observe that the relevant vectorial structure of the frequency shifts (49), (50), (52) and (53) depends only on the moduli of the dipole moments components meaning that they will contribute to the whole quantities given in Eqs. (32) and (33) no matter whether the dipole moments are real or complex. This reflects that the perfectly conducting mirror and its corresponding dipole moments do not exhibit parity breaking or time-reversal symmetry

breaking, i.e., they are P -even and T -even. In Table I we resume the behavior that a perfectly conducting mirror and its dipole moments \mathbf{d}_{nk} must have under P and T transformations. Meanwhile, the shift (51) and (54) are governed by

$$S_{nk}(\mathbf{v}_{\parallel}) = \text{Im} [(\mathbf{d}_{nk}^* \cdot \mathbf{e}_z) (\mathbf{d}_{nk} \cdot \mathbf{v}_{\parallel})] = 0, \quad (55)$$

which has the same units as the optical rotatory strength found in chiral molecules [59, 60] but is a vanishing quantity because Maxwell equations require that $\mathbf{v}_{\parallel} \cdot \mathbf{d}_{nk} = 0$ so the P -even and T -even behavior of this material is respected. Lastly, we remark that due to our approximation at first order in v/c , the sign of the velocity could lead to an increase or decrease in the velocity-dependent frequency shifts.

B. Perfectly reflecting nonreciprocal mirror

This mirror is characterized by vanishing polarization preserving reflection coefficients for incoming perpendicular or parallel polarization and outgoing perpendicular or parallel polarization $r_{s,s} = r_{p,p} = 0$ and therefore the mixing terms $r_{p,s}$ and $r_{s,p}$ can be chosen to be either ± 1 [64, 71]. We will restrict ourselves to the case $r_{p,s} = r_{s,p} = -1$. Under these conditions the Green's tensor (44) results antisymmetric $\mathbb{G}^{(1)\top}(\mathbf{r}, \mathbf{r}'; \omega) = -\mathbb{G}^{(1)}(\mathbf{r}', \mathbf{r}; \omega)$ whose only nonzero components are [64]

$$\mathbb{G}_{xy}^{(1)}(\mathbf{r}, \mathbf{r}; \omega) = \left(-\frac{1}{8\pi z} - \frac{ic}{16\pi\omega z^2} \right) e^{\frac{2i\omega z}{c}}, \quad (56)$$

$$\mathbb{G}_{yx}^{(1)}(\mathbf{r}, \mathbf{r}; \omega) = -\mathbb{G}_{xy}^{(1)}(\mathbf{r}, \mathbf{r}; \omega). \quad (57)$$

The contributions to the frequency shift (33) for the dipole (45) in the retarded limit ($\tilde{\omega}_{nk}z_A/c \gg 1$) read as follows

$$\delta\omega_{nk}^{\text{res,ret}}(\mathbf{r}_A) = -\frac{\mu_0\tilde{\omega}_{nk}^2\mathcal{B}_z}{4\pi\hbar z_A} \sin\left(\frac{2\tilde{\omega}_{nk}z_A}{c}\right), \quad (58)$$

$$\delta\omega_{nk}^{\text{nres,ret}}(\mathbf{r}_A) = -\frac{3c^2\mathcal{B}_z}{32\pi^2\hbar\varepsilon_0\tilde{\omega}_{nk}^2z_A^5}, \quad (59)$$

$$\delta\omega_{nk}^{\text{ret}}(\mathbf{r}_A, \mathbf{v}) = \frac{\mu_0\tilde{\omega}_{nk}^2}{4\pi\hbar cz_A} T_{nk}(\mathbf{v}_{\parallel}) \cos\left(\frac{2\tilde{\omega}_{nk}z_A}{c}\right), \quad (60)$$

where the dominating contribution to the frequency shift (60) comes from the electric interaction $\mathbf{d}_{mn} \cdot \hat{\mathbf{E}}(\mathbf{r}_A)$. For the nonretarded limit ($\tilde{\omega}_{nk}z_A/c \ll 1$), we find

$$\delta\omega_{nk}^{\text{res,nret}}(\mathbf{r}_A) = -\frac{\mu_0 c \tilde{\omega}_{nk}}{8\pi\hbar z_A^2} \mathcal{B}_z, \quad (61)$$

$$\delta\omega_{nk}^{\text{nres,nret}}(\mathbf{r}_A) = -\frac{\mathcal{B}_z}{16\pi^2\hbar\varepsilon_0 z_A^3}, \quad (62)$$

$$\delta\omega_{nk}^{\text{nret}}(\mathbf{r}_A, \mathbf{v}) = -\frac{T_{nk}(\mathbf{v}_{\parallel})}{16\pi\hbar\varepsilon_0 cz_A^3}. \quad (63)$$

For this mirror, we identify that the relevant vectorial structure of Eqs. (58), (59), (61) and (62), depends on

$$\mathcal{B}_z = \text{Im}(d_{nk}^x d_{nk}^{y*}) = \frac{1}{2i} (\mathbf{d}_{nk} \times \mathbf{d}_{nk}^*) \cdot \mathbf{e}_z, \quad (64)$$

which is T -odd and shows that \mathbf{d}_{nk} , \mathbf{d}_{nk}^* and \mathbf{e}_z must not be coplanar. In this way, the time-reversal symmetry breaking for such position-dependent quantities becomes explicitly manifest in comparison with the previous study [64] because only circular or elliptical polarizations parallel to the xy plane will give a non-zero contribution. In other words, linear polarizations are ruled out because they give $\mathbf{d}_{nk} \times \mathbf{d}_{nk}^* = \mathbf{0}$ as a consequence of their invariance under time-reversal symmetry and colinearity. Important to highlight is the cross product of Eq. (64), which in the framework of chiral media can be understood as a geometric magnetic field \mathcal{B} associated with photoionization of chiral molecules [72, 73] and whose z component is the only relevant here. This offers another first connection between the physics of chirality and nonreciprocity.

On the other hand, Eqs. (60) and (63) share the same vectorial structure for the atomic response

$$T_{nk}(\mathbf{v}_{\parallel}) = \text{Re} \{ (\mathbf{d}_{nk}^* \cdot \mathbf{e}_z) [(\mathbf{v}_{\parallel} \times \mathbf{d}_{nk}) \cdot \mathbf{e}_z] \}, \quad (65)$$

which is T -odd and does not vanish if \mathbf{v}_{\parallel} , \mathbf{d}_{nk} and \mathbf{e}_z are not coplanar and if $d_{nk}^z \neq 0$. These conditions imply the necessity of a superposition of linear polarizations to obtain a non-zero contribution for the velocity-dependent quantities opposed to what the position-dependent ones required via \mathcal{B}_z (64). Besides $d_{nk}^z \neq 0$ this vectorial structure needs either $d_{nk}^x \neq 0$ or $d_{nk}^y \neq 0$, which results in the surprising possibility to turn off only the position-dependent of Eqs. (58), (59), (61) and (62). Namely, if we choose the polarized dipole in the xz plane $\mathbf{d}_{nk} = d_{nk}/\sqrt{2}(0, 1, 1)^\top$, for which $d_{nk}^x = 0$, then Eq. (64) is zero but $\text{Re} \{ (\mathbf{d}_{nk}^* \cdot \mathbf{e}_z) [(\mathbf{v}_{\parallel} \times \mathbf{d}_{nk}) \cdot \mathbf{e}_z] \} \neq 0$ leading to non-zero velocity-dependent quantities.

Given the important role of such vectorial structure, let us inspect its origin. In this way, we recall the interaction Hamiltonian and regard only the Röntgen interaction, which can be rewritten as shown:

$$\hat{H}_{\text{Röntgen}} = \mathbf{v} \cdot \hat{\mathbf{d}} \times \hat{\mathbf{B}}(\mathbf{r}_A) = -\hat{\mathbf{m}} \cdot \hat{\mathbf{B}}(\mathbf{r}_A), \quad (66)$$

where

$$\hat{\mathbf{m}} = -\mathbf{v} \times \hat{\mathbf{d}}. \quad (67)$$

This means that an effective magnetic moment is induced. In this way, the vectorial structure for the velocity-dependent quantities takes the following fashion

$$\begin{aligned} \text{Re} \{ (\mathbf{d}_{nk}^* \cdot \mathbf{e}_z) [(\mathbf{v}_{\parallel} \times \mathbf{d}_{nk}) \cdot \mathbf{e}_z] \} &= -\text{Re}(d_{nk}^{z*} m_{nk}^z), \\ &= T_{nk}(\mathbf{v}_{\parallel}), \end{aligned} \quad (68)$$

which resembles the optical rotatory strength $R_{nk} = -\text{Im}(d_{nk}^{z*} \cdot m_{nk})$ of chiral molecules [59, 60] but this one

Medium	P	T	Atom	P	T	$\delta\omega_{nk}$
Perfectly conducting mirror	+	+	$ \mathbf{d}_{nk} ^2$	+	+	+
Nonreciprocal mirror	-	-	$\mathcal{B}_z, T_{nk}(\mathbf{v}_{\parallel})$	-	-	+
3D topological insulator	-	-	$\mathcal{B}_z, T_{nk}(\mathbf{v}_{\parallel})$	-	-	+
Chiral mirror	-	+	$R_{nk}(\mathbf{v}_{\parallel})$	-	+	+
Isotropic chiral medium	-	+	$R_{nk}(\mathbf{v}_{\parallel})$	-	+	+

TABLE I: Behavior under parity P and time-reversal T of the five media considered in this work and their atomic electric dipole \mathbf{d}_{nk} and its corresponding medium. The second and third columns display the behavior under P and T of the five materials. Each medium is coupled to an atomic response whose behavior under P and T is shown in the fourth and fifth columns. The last column shows that the coupling of each material with its atomic response gives a P - and T - even frequency shift. \mathcal{B}_z is given by Eq. (64), $T_{nk}(\mathbf{v}_{\parallel})$ is defined in Eq. (68) and $R_{nk}(\mathbf{v}_{\parallel})$ in Eq. (91).

needs the real part implying the necessity of real dipoles. The form of $T_{nk}(\mathbf{v}_{\parallel})$ is in agreement with the Casimir–Polder potential perspective studied on Ref. [71], where for nonreciprocal media it is required that $\mathbf{d}_{nk} \otimes \mathbf{m}_{kn}$ must be real as part of the crossed polarisability. In order to distinguish between the nonreciprocal and the ordinary rotatory strengths, we will name $T_{nk}(\mathbf{v}_{\parallel})$ as nonreciprocal optical rotatory strength. This constitutes the second connection found in this work between the physics of chirality and nonreciprocity. In Table I we resume the behavior that a perfectly reflecting nonreciprocal mirror and its dipole moments \mathbf{d}_{nk} must have under P and T transformations.

Our two final remarks for this section are as follows. First, without velocity the nonreciprocal optical rotatory strength T_{nk} is zero, thus there is no magnetic moment so the whole velocity-dependent effect is zero. And second, due to our approximation at first order in v/c , the sign of the velocity could lead to an increase or decrease in the velocity-dependent frequency shifts as happened to the perfectly conducting mirror discussed in the previous subsection.

C. 3D topological insulator

For these materials, the electric and magnetic field are connected with the displacement field $\hat{\mathbf{D}}(\mathbf{r};\omega)$ and the magnetic field $\hat{\mathbf{H}}(\mathbf{r};\omega)$ via

$$\hat{\mathbf{D}}(\mathbf{r};\omega) = \varepsilon_0\varepsilon(\mathbf{r};\omega)\hat{\mathbf{E}}(\mathbf{r};\omega) + \frac{\alpha\Theta(\mathbf{r};\omega)}{\pi\mu_0c}\hat{\mathbf{B}}(\mathbf{r};\omega) + \hat{\mathbf{P}}_N(\mathbf{r};\omega), \quad (69)$$

$$\hat{\mathbf{H}}(\mathbf{r};\omega) = \frac{\hat{\mathbf{B}}(\mathbf{r};\omega)}{\mu_0\mu(\mathbf{r};\omega)} - \frac{\alpha\Theta(\mathbf{r};\omega)}{\pi\mu_0c}\hat{\mathbf{E}}(\mathbf{r};\omega) - \hat{\mathbf{M}}_N(\mathbf{r};\omega), \quad (70)$$

where α is the fine structure constant and $\varepsilon(\mathbf{r};\omega)$, $\mu(\mathbf{r};\omega)$, and $\Theta(\mathbf{r};\omega)$ are the dielectric permittivity, magnetic permeability, and axion coupling, respectively. Here the $\hat{\mathbf{P}}_N(\mathbf{r};\omega)$ and $\hat{\mathbf{M}}_N(\mathbf{r};\omega)$ terms are the noise polarization and magnetization, respectively. These are Langevin noise terms that model absorption within the

material [74]. The axion coupling $\Theta(\mathbf{r};\omega)$ takes even multiples of π in weak three-dimensional TIs and odd multiples of π in strong three-dimensional TIs, with the magnitude and sign of the multiple given by the strength and direction of the time-symmetry-breaking perturbation. Although, the weak class of TIs is under active research it provides more complications because lattice translation symmetry together with time-reversal symmetry protect the conducting states at the boundaries of a weak 3D TI, which requires to take into account also disorder and anisotropies Ref. [36, 75, 76]. For these reasons, in this work we will only consider the strong class of them. When Θ is restricted to a nondynamical field, the theory is usually referred as Θ -Electrodynamics [48, 77, 78], which has the necessary topological features to model the electromagnetic behavior of strong 3D TIs [46] and also naturally existing magnetoelectric media [79, 80] such as Cr_2O_3 with $\Theta \simeq \pi/36$ [44, 81].

The modified Fresnel reflective coefficients for nonreciprocal media $r_{\sigma,\sigma'}$ involved in Eq. (44) can be derived from the application of the boundary conditions to above constitutive relations. These reflective coefficients can be found in Ref. [70] in its general form. However, we will particularize them for the case of an interface constituted by vacuum in the upper layer of Fig. 1 and a strong three-dimensional TI with real permittivity in the lower layer as shown

$$r_{s,s} = \frac{(\mu_2 k_1^\perp - k_2^\perp)\mu_2(\varepsilon_2 k_1^\perp + k_2^\perp) - \Delta^2 k_1^\perp k_2^\perp}{(\mu_2 k_1^\perp + k_2^\perp)\mu_2(\varepsilon_2 k_1^\perp + k_2^\perp) + \Delta^2 k_1^\perp k_2^\perp}, \quad (71)$$

$$r_{s,p} = \frac{-2\mu_2 k_1^\perp k_2^\perp \Delta}{(\mu_2 k_1^\perp + k_2^\perp)\mu_2(\varepsilon_2 k_1^\perp + k_2^\perp) + \Delta^2 k_1^\perp k_2^\perp}, \quad (72)$$

$$r_{p,p} = \frac{(\varepsilon_2 k_1^\perp - k_2^\perp)\mu_2(\mu_2 k_1^\perp + k_2^\perp) + \Delta^2 k_1^\perp k_2^\perp}{(\mu_2 k_1^\perp + k_2^\perp)\mu_2(\varepsilon_2 k_1^\perp + k_2^\perp) + \Delta^2 k_1^\perp k_2^\perp}, \quad (73)$$

$$r_{p,s} = r_{s,p}, \quad (74)$$

where the subscript 1 denotes the corresponding quantities in the vacuum and conversely the subscript 2 for the strong 3D TI. The perpendicular part of the wave vector is denoted by k_1^\perp and k_2^\perp for the corresponding medium. For the general case when two semi-infinite magnetoelectric media with different axion couplings constitute the planar interface, the topological parameter Δ takes the

following form [70]

$$\Delta = \alpha\mu_1\mu_2(\Theta_2 - \Theta_1)/\pi. \quad (75)$$

Nevertheless, for the selected interface the strong 3D TI with $\Theta_1 = \pi$ and vacuum with $\Theta_2 = 0$, the topological parameter takes the next form

$$\Delta = \alpha(2m + 1), \quad (76)$$

where m is an integer depending on the details of the time-reversal-symmetry breaking at the interface.

The contributions to the frequency shift (33) for the dipole (45) in the retarded limit ($\tilde{\omega}_{nk}z_A/c \gg 1$) read as follows

$$\begin{aligned} \delta\omega_{nk}^{\text{res,ret}}(\mathbf{r}_A) &= \frac{\mu_0\tilde{\omega}_{nk}^2}{4\pi\hbar} \left[\mathcal{B}_z \frac{r_{\text{s,p}}^{\text{ret}}}{z_A} \sin\left(\frac{2\tilde{\omega}_{nk}z_A}{c}\right) \right. \\ &\quad + |\mathbf{d}_{nk}^{\parallel}|^2 \frac{r_{\text{p,p}}^{\text{ret}}}{2z_A} \cos\left(\frac{2\tilde{\omega}_{nk}z_A}{c}\right) \\ &\quad \left. - \frac{c r_{\text{p,p}}^{\text{ret}} |d_{nk}^z|^2}{2\tilde{\omega}_{nk}z_A^2} \sin\left(\frac{2\tilde{\omega}_{nk}z_A}{c}\right) \right], \quad (77) \end{aligned}$$

$$\begin{aligned} \delta\omega_{nk}^{\text{nres,ret}}(\mathbf{r}_A) &= \frac{c}{32\pi^2\hbar\varepsilon_0\tilde{\omega}_{nk}z_A^4} \left[\mathcal{B}_z \frac{3c r_{\text{s,p}}^{\text{ret}}}{\tilde{\omega}_{nk}z_A} \right. \\ &\quad \left. + r_{\text{p,p}}^{\text{ret}} |\mathbf{d}_{nk}^{\parallel}|^2 \right], \quad (78) \end{aligned}$$

$$\delta\omega_{nk}^{\text{ret}}(\mathbf{r}_A, \mathbf{v}) = \frac{\mu_0\tilde{\omega}_{nk}^2}{4\pi\hbar cz_A} r_{\text{s,p}}^{\text{ret}} T_{nk}(\mathbf{v}_{\parallel}) \cos\left(\frac{2\tilde{\omega}_{nk}z_A}{c}\right), \quad (79)$$

where $S_{nk}(\mathbf{v}_{\parallel}) = 0$ from Eq. (55) was used and the nonreciprocal optical rotatory strength $T_{nk}(\mathbf{v}_{\parallel})$ was defined in Eq. (68), and both of them will be subsequently employed. The retarded limit of the Fresnel coefficients are given in Appendix A. Again, the dominating contribution to the frequency shift (79) comes from the electric interaction $\mathbf{d}_{mn} \cdot \hat{\mathbf{E}}(\mathbf{r}_A)$ as in the nonreciprocal mirror. For the nonretarded limit ($\tilde{\omega}_{nk}z_A/c \ll 1$), we obtain

$$\begin{aligned} \delta\omega_{nk}^{\text{res,nret}}(\mathbf{r}_A) &= \frac{\mu_0\tilde{\omega}_{nk}^2}{8\pi\hbar} \left[\mathcal{B}_z \frac{r_{\text{s,p}}^{\text{nret}} c}{\tilde{\omega}_{nk}z_A^2} \right. \\ &\quad \left. + |\mathbf{d}_{nk}^{\parallel}|^2 \left(\frac{r_{\text{s,s}}^{\text{nret}}}{2z_A} + \frac{r_{\text{p,p}}^{\text{nret}} c^2}{\tilde{\omega}_{nk}^2 z_A^3} \right) + \frac{c^2 r_{\text{p,p}}^{\text{nret}} |d_{nk}^z|^2}{2\tilde{\omega}_{nk}^2 z_A^3} \right], \quad (80) \end{aligned}$$

$$\begin{aligned} \delta\omega_{nk}^{\text{nres,nret}}(\mathbf{r}_A) &= \frac{1}{16\pi^2\hbar\varepsilon_0 z_A^3} \left[\mathcal{B}_z r_{\text{s,p}}^{\text{nret}} \right. \\ &\quad \left. + r_{\text{p,p}}^{\text{nret}} \pi \left(\frac{|\mathbf{d}_{nk}^{\parallel}|^2}{4} + \frac{|d_{nk}^z|^2}{2} \right) \right], \quad (81) \end{aligned}$$

$$\delta\omega_{nk}^{\text{nret}}(\mathbf{r}_A, \mathbf{v}) = \frac{r_{\text{s,p}}^{\text{nret}} T_{nk}(\mathbf{v}_{\parallel})}{16\pi\hbar\varepsilon_0 c z_A^3}, \quad (82)$$

where the nonretarded limit of the Fresnel coefficients are given in Appendix A.

For the strong 3D TI, we observe that the resulting frequency shifts are a superposition of the corresponding

quantities of the perfectly conducting mirror of Sec. IV A and the perfectly reflecting nonreciprocal mirror of Sec. IV B determined by the Fresnel coefficients $r_{\sigma,\sigma'}$. As a result, all the previous discussions and mainly the conditions over \mathbf{v}_{\parallel} , \mathbf{d}_{nk} and \mathbf{e}_z discussed previously apply. Moreover, the reflective coefficients are functions of the permittivity ε and the topological parameter Δ which could help to modulate the behavior of the spectroscopical quantities. For instance, we could increase Δ by substituting the strong 3D TI by a magnetoelectric like TbPO_4 with $\varepsilon_2 = 3.4969$, $\mu_2 = 1$, and $\Delta = 0.22$ [82, 83]. Similarly to the sign of the velocity discussed for the perfectly conducting and the nonreciprocal mirror, the topological parameter Δ can acquire a different sign for certain strong 3D TIs. This can be easily seen from the crossed reflective coefficients in Appendix A which are proportional to Δ in the retarded and the nonretarded limits. This would lead to an increase or decrease the corresponding contribution. However, the whole frequency shift is T -even once T is applied to $T_{nk}(\mathbf{v}_{\parallel})$. In Table I we resume the behavior that a strong 3D TI and its dipole moments \mathbf{d}_{nk} must have under P and T transformations, where both atom and medium are falsely chiral. Furthermore, due to the internal connection between the frequency shift and the Casimir-Polder force, one can also be able to switch from an attractive to a repulsive force between atom and medium. Notwithstanding this possibility, an extremely large axion coupling will approximate these results to those of the perfectly conducting mirror because in that limit $r_{\text{p,s}} = r_{\text{s,p}} \rightarrow 0$, $r_{\text{s,s}} \rightarrow -1$ and $r_{\text{p,p}} \rightarrow 1$ as discussed in Ref. [64].

D. Perfectly reflecting chiral mirror

Now we proceed towards chiral media. Although this kind of media are reciprocal meaning that they verify the Lorentz reciprocity principle for the Green's tensor $\mathbb{G}(\mathbf{r}, \mathbf{r}'; \omega) = \mathbb{G}^{\text{T}}(\mathbf{r}', \mathbf{r}; \omega)$ [60, 84, 85], our result for the velocity-dependent frequency shift (37) shows that the curl of the Green's tensor must not be zero. This feature is indeed satisfied by chiral media [60] justifying such choice. At this point we remark that the application of our results for chiral media will only need to employ $\mathbb{G}(\mathbf{r}, \mathbf{r}'; \omega) = \mathbb{G}^{\text{T}}(\mathbf{r}', \mathbf{r}; \omega)$ in all the required formulae, which means clearly that chiral media are a particular case of nonreciprocal media. The resulting expressions are

$$\begin{aligned} \delta\omega_{nk}(\mathbf{r}_A, \mathbf{v}) &= \\ &\frac{\mu_0}{\hbar} \left\{ \omega^2 \text{Im} \left[\mathbf{d}_{kn} \cdot (\mathbf{v} \cdot \nabla') \mathbb{G}^{(1)}(\mathbf{r}_A, \mathbf{r}_A; \omega) \cdot \mathbf{d}_{nk} \right] \right\}'_{\omega=\tilde{\omega}_{nk}} \\ &\quad - \frac{\mu_0}{\hbar} \tilde{\omega}_{nk} \text{Im} \left\{ \mathbf{v} \cdot \mathbf{d}_{kn} \times \left[\nabla \times \mathbb{G}^{(1)}(\mathbf{r}_A, \mathbf{r}_A; \tilde{\omega}_{nk}) \right] \cdot \mathbf{d}_{nk} \right\} \\ &\quad + \frac{\mu_0}{\hbar} \tilde{\omega}_{nk} \text{Im} \left\{ \mathbf{v} \cdot \mathbf{d}_{nk} \times \left[\nabla \times \mathbb{G}^{(1)}(\mathbf{r}_A, \mathbf{r}_A; \tilde{\omega}_{nk}) \right] \cdot \mathbf{d}_{kn} \right\}, \quad (83) \end{aligned}$$

and the quantities given by Eqs. (42) and (43) remain the same.

Let us begin with the perfectly reflecting chiral mirror. In contrast with the perfectly conducting mirror of Sec. IV A and the nonreciprocal mirror of Sec. IV B, a perfect chiral mirror has the mixing terms $r_{p,s} = -r_{s,p} = \pm i$ and therefore $r_{s,s} = r_{p,p} = 0$ [54]. Here we adopt the convention that a left-handed mirror or a mirror of positive chirality rotates the polarization of an electromagnetic wave in a counterclockwise direction upon reflection when traveling alongside the wave defining the reflection coefficients $r_{p,s} = -r_{s,p} = i$, whereas a right-handed mirror of negative chirality rotates it in a clockwise direction specified by the $r_{p,s} = -r_{s,p} = -i$. Under these conditions the Green's tensor (44) results [60]

$$\mathbb{G}^{(1)}(\mathbf{r}, \mathbf{r}'; \omega) = \frac{ic}{8\pi^2\omega} \int \frac{d^2\mathbf{k}_\parallel}{k_\perp} e^{i\mathbf{k}_\parallel \cdot (\mathbf{r}-\mathbf{r}')} e^{ik_\perp(z+z')} \times (r_{s,p}\mathbf{e}_s \otimes \mathbf{e}_{p-} + r_{p,s}\mathbf{e}_{p+} \otimes \mathbf{e}_s), \quad (84)$$

The contributions to the frequency shift (33) for the dipole (45) in the retarded limit ($\tilde{\omega}_{nk}z_A/c \gg 1$) read as follows

$$\delta\omega_{nk}^{\text{res,ret}}(\mathbf{r}_A) = 0, \quad (85)$$

$$\delta\omega_{nk}^{\text{nres,ret}}(\mathbf{r}_A) = 0. \quad (86)$$

$$\delta\omega_{nk}^{\text{ret}}(\mathbf{r}_A, \mathbf{v}) = \pm \frac{\tilde{\omega}_{nk}^2 R_{nk}(\mathbf{v}_\parallel)}{4\pi\hbar\varepsilon_0 c^2 z_A} \cos\left(\frac{2\tilde{\omega}_{nk}z_A}{c}\right), \quad (87)$$

where the dominating contribution to the frequency shift (87) comes from the electric interaction $\mathbf{d}_{mn} \cdot \hat{\mathbf{E}}(\mathbf{r}_A)$ as in the nonreciprocal media. For the nonretarded limit ($\tilde{\omega}_{nk}z_A/c \ll 1$), we find

$$\delta\omega_{nk}^{\text{res,nret}}(\mathbf{r}_A) = 0, \quad (88)$$

$$\delta\omega_{nk}^{\text{nres,nret}}(\mathbf{r}_A) = 0, \quad (89)$$

$$\delta\omega_{nk}^{\text{nret}}(\mathbf{r}_A, \mathbf{v}) = \mp \frac{R_{nk}(\mathbf{v}_\parallel)}{8\pi\hbar\varepsilon_0 c z_A^3}. \quad (90)$$

For this mirror, we observe that all the position-dependent spectroscopical quantities are zero. This is explained by means of the Curie's principle [69] mentioned in Sec. III, which applied for this situation establishes the necessity of a chiral source to probe the chirality of the mirror. This means that we need not only an electric dipole but also a magnetic dipole, for which our effective magnetic dipole of Eq. (67) does not work because velocities are not taken into account by the position-dependent frequency shifts (42) and (43). This can be traced back to the origin of these quantities that arise only from the electric dipole interaction of the interaction Hamiltonian given in Eq. (9).

In spite of that, all velocity-dependent quantities are nonzero because now due to our effective magnetic dipole (67) as well as the electric dipole serve to probe the chirality of the mirror leading to nonzero results. All these quantities depend on

$$\begin{aligned} R_{nk}(\mathbf{v}_\parallel) &= \text{Im} \left\{ (\mathbf{d}_{nk}^* \cdot \mathbf{e}_z) [(\mathbf{v}_\parallel \times \mathbf{d}_{nk}) \cdot \mathbf{e}_z] \right\}, \\ &= -\text{Im} (d_{nk}^{z*} m_{nk}^z), \end{aligned} \quad (91)$$

where we identified in the last line the optical rotatory strength by means of the Röntgen interaction Hamiltonian (66) being a P -odd quantity appearing naturally for any chiral molecule [59, 60]. Therefore, we can interpret that an effective circular dichroism of the transition $n \leftarrow k$ between the electric dipole and the effective magnetic moment of Eq. (67). This means that we are observing motion-induced chirality.

Because the optical rotatory strength $R_{nk}(\mathbf{v}_\parallel)$ (91) is a pure imaginary number, it needs circularly or elliptical polarized dipoles, which contrast strongly with the required ones for its nonreciprocal counterpart (68). Due to its vectorial structure the non coplanarity condition over \mathbf{v}_\parallel , \mathbf{d}_{nk} and \mathbf{e}_z and the condition $\mathbf{v}_\parallel \cdot \mathbf{d}_{nk} = 0$ discussed previously are valid. The form of $R_{nk}(\mathbf{v}_\parallel)$ (91) is in agreement with the Casimir-Polder potential perspective studied on Ref. [71], where for chiral media it is required that $\mathbf{d}_{nk} \otimes \mathbf{m}_{kn}$ must be a pure imaginary number as part of the crossed polarisability. In Table I we resume the behavior that a perfectly reflecting chiral mirror and its dipole moments \mathbf{d}_{nk} must have under P and T transformations.

Similarly to our discussion for the previous nonreciprocal materials, we also observe that these quantities could increase or decrease the corresponding contribution depending on which handedness for the mirror is used. This is a big difference with the nonreciprocal mirror of Sec. IV B, whose quantities lack this freedom. Our final comment for this Section is that the frequency shift of Eq. (90) reproduces the z^{-3} dependence of Ref. [70] obtained through perturbation theory for the circularly polarized dipole $\mathbf{d}_{nk} = d_{nk}/\sqrt{2}(0, 1, i)^\top$.

E. Isotropic Chiral medium

For these materials, the electric and magnetic field are connected with the displacement field $\hat{\mathbf{D}}(\mathbf{r}; \omega)$ and the magnetic field $\hat{\mathbf{H}}(\mathbf{r}; \omega)$ via the Boys-Post constitutive relationships [60, 63, 86, 87]

$$\begin{aligned} \hat{\mathbf{D}}(\mathbf{r}; \omega) &= \varepsilon_0 \varepsilon(\mathbf{r}; \omega) \hat{\mathbf{E}}(\mathbf{r}; \omega) - \frac{i\kappa}{c} \hat{\mathbf{H}}(\mathbf{r}; \omega) \\ &\quad + \hat{\mathbf{P}}_N(\mathbf{r}; \omega) - \frac{i\kappa}{c} \hat{\mathbf{M}}_N, \end{aligned} \quad (92)$$

$$\begin{aligned} \hat{\mathbf{B}}(\mathbf{r}; \omega) &= \mu_0 \mu(\mathbf{r}; \omega) \hat{\mathbf{H}}(\mathbf{r}; \omega) + \frac{i\kappa}{c} \hat{\mathbf{E}}(\mathbf{r}; \omega) \\ &\quad + \mu_0 \mu(\mathbf{r}; \omega) \hat{\mathbf{M}}_N(\mathbf{r}; \omega), \end{aligned} \quad (93)$$

where κ is the chiral cross-susceptibility, a magnetoelectric susceptibility being in general a tensor. The chiral cross-susceptibility of the medium has the effect of "rotating" a magnetic effect to contribute towards an electric response and vice versa. The similarities and differences between the above constitutive relations and those for the 3D TI dictated by Eqs. (69) and (70) can be discussed from a truly and falsely chiral perspective [51, 88, 89]:

in this context, the above chiral medium is truly chiral, while the 3D TI is falsely chiral [90].

The modified Fresnel reflective coefficients for nonreciprocal media $r_{\sigma,\sigma'}$ involved in Eq. (44) can be found in Ref. [84] in its general form. Nevertheless, we will particularize them for the case of an interface constituted by vacuum in the upper half-space of Fig. 1 and an isotropic chiral medium in the lower half-space. By employing the same notation of Sec. IV C where subscript 1 denotes the corresponding quantities in the vacuum and conversely the subscript 2 for the chiral medium, we have

$$r_{s,s} = \frac{1}{\mathcal{D}} [(1 + a_R)(1 - b_L) + (1 + a_L)(1 - b_R)], \quad (94)$$

$$r_{s,p} = \frac{-2ik_1}{\mathcal{D}k_1^\perp} \left(\frac{k_2^{\perp,L}}{k_2^L} - \frac{k_2^{\perp,R}}{k_2^R} \right), \quad (95)$$

$$r_{p,p} = \frac{1}{\mathcal{D}} [(1 - a_R)(1 + b_L) + (1 - a_L)(1 + b_R)], \quad (96)$$

$$r_{p,s} = -r_{s,p}, \quad (97)$$

where $\mathcal{D} = (1 + a_R)(1 + b_L) + (1 + a_L)(1 + b_R)$ and

$$a_P = \frac{\sqrt{\varepsilon_2}k_1k_2^{\perp,P}}{\sqrt{\mu_2}k_1^\perp k_2^P}, \quad b_P = \frac{\sqrt{\mu_2}k_1k_2^{\perp,P}}{\sqrt{\varepsilon_2}k_1^\perp k_2^P}, \quad (98)$$

with P = R,L referring to the right and left circular polarization of the wave, respectively. Within the chiral medium the wave vectors are

$$(k_2^R)^2 = \frac{\omega^2}{c^2} (\sqrt{\varepsilon_2\mu_2} + \kappa_2)^2, \quad (99)$$

$$(k_2^L)^2 = \frac{\omega^2}{c^2} (\sqrt{\varepsilon_2\mu_2} - \kappa_2)^2, \quad (100)$$

$$(k_2^{\perp,P})^2 = (k_2^P)^2 - (k_2^\parallel)^2. \quad (101)$$

For the vacuum, which is at the achiral region 1 the wave vectors are the standard free-space ones

$$k_1 = \frac{\omega}{c}, \quad (k_1^\perp)^2 = k_1^2 - (k_1^\parallel)^2, \quad (102)$$

where $k^\parallel = k_x^2 + k_y^2$.

The contributions to the frequency shift (33) for the dipole (45) in the retarded limit ($\tilde{\omega}_{nk}z_A/c \gg 1$) read as follows

$$\begin{aligned} \delta\omega_{nk}^{\text{res,ret}}(\mathbf{r}_A) &= \frac{\mu_0\tilde{\omega}_{nk}^2|\mathbf{d}_{nk}^\parallel|^2}{16\pi\hbar z_A} \\ &\times \left[\cos\left(\frac{2\tilde{\omega}_{nk}z_A}{c}\right) \text{Re}(r_{p,p}^{\text{ret}} - r_{s,s}^{\text{ret}}) \right. \\ &+ \left. \sin\left(\frac{2\tilde{\omega}_{nk}z_A}{c}\right) \text{Im}(r_{p,p}^{\text{ret}} - r_{s,s}^{\text{ret}}) \right] \\ &- \frac{\mu_0\tilde{\omega}_{nk}|d_{nk}^z|^2}{8\pi\hbar cz_A^2} \left[\text{Re}(r_{p,p}^{\text{ret}}) \sin\left(\frac{2\tilde{\omega}_{nk}z_A}{c}\right) \right. \\ &+ \left. \text{Im}(r_{p,p}^{\text{ret}}) \cos\left(\frac{2\tilde{\omega}_{nk}z_A}{c}\right) \right], \quad (103) \end{aligned}$$

$$\begin{aligned} \delta\omega_{nk}^{\text{nres,ret}}(\mathbf{r}_A) &= \frac{c^2}{32\pi^2\hbar\varepsilon_0\tilde{\omega}_{nk}z_A^5} \\ &\times \left[\frac{|\mathbf{d}_{nk}^\parallel|^2}{4} \text{Im}(r_{s,s}^{\text{ret}} - r_{p,p}^{\text{ret}}) - |d_{nk}^z|^2 \text{Im}(r_{p,p}^{\text{ret}}) \right] \\ &- \frac{c}{32\pi^2\hbar\varepsilon_0\tilde{\omega}_{nk}z_A^4} \left[\frac{|\mathbf{d}_{nk}^\parallel|^2}{2} \text{Re}(r_{s,s}^{\text{ret}} - r_{p,p}^{\text{ret}}) \right. \\ &- \left. |d_{nk}^z|^2 \text{Re}(r_{p,p}^{\text{ret}}) \right], \quad (104) \end{aligned}$$

$$\begin{aligned} \delta\omega_{nk}^{\text{ret}}(\mathbf{r}_A, \mathbf{v}) &= \frac{\tilde{\omega}_{nk}^2 R_{nk}(\mathbf{v}_\parallel)}{4\pi\hbar\varepsilon_0 c^2 z_A} \left[\text{Re}(r_{s,p}^{\text{ret}}) \sin\left(\frac{2\tilde{\omega}_{nk}z_A}{c}\right) \right. \\ &+ \left. \text{Im}(r_{s,p}^{\text{ret}}) \cos\left(\frac{2\tilde{\omega}_{nk}z_A}{c}\right) \right], \quad (105) \end{aligned}$$

where $S_{nk}(\mathbf{v}_\parallel) = 0$ from Eq. (55) was used and the optical rotatory strength $R_{nk}(\mathbf{v}_\parallel)$ was defined in Eq. (91), and both of them will be subsequently employed. In this limit, we found that for $\kappa \in \mathbb{C}$, $r_{s,p}^{\text{ret}}$ will not vanish. For this reason, we consider the more general case of $\varepsilon, \kappa \in \mathbb{C}$ to analyze the chiral effects in this retarded limit. The retarded limit of the Fresnel coefficients are given in Appendix B. Again, the dominating contribution to the frequency shift (105) comes from the electric interaction $\mathbf{d}_{mn} \cdot \hat{\mathbf{E}}(\mathbf{r}_A)$ as in the nonreciprocal media and the perfectly chiral mirror. For the nonretarded limit ($\tilde{\omega}_{nk}z_A/c \ll 1$), we obtain

$$\begin{aligned} \delta\omega_{nk}^{\text{res,nret}}(\mathbf{r}_A) &= \frac{\mu_0\tilde{\omega}_{nk}^2}{8\pi\hbar} \left[|\mathbf{d}_{nk}^\parallel|^2 \left(\frac{r_{s,s}^{\text{nret}}}{2z_A} + \frac{r_{p,p}^{\text{nret}}c^2}{\tilde{\omega}_{nk}^2 z_A^3} \right) \right. \\ &+ \left. \frac{c^2 r_{p,p}^{\text{nret}} |d_{nk}^z|^2}{2\tilde{\omega}_{nk}^2 z_A^3} \right], \quad (106) \end{aligned}$$

$$\delta\omega_{nk}^{\text{nres,nret}}(\mathbf{r}_A) = \frac{r_{p,p}^{\text{nret}}}{16\pi\hbar\varepsilon_0 z_A^3} \left(\frac{|\mathbf{d}_{nk}^\parallel|^2}{4} + \frac{|d_{nk}^z|^2}{2} \right), \quad (107)$$

$$\delta\omega_{nk}^{\text{nret}}(\mathbf{r}_A, \mathbf{v}) = \frac{R_{kn} \text{Im}(r_{s,p}^{\text{nret}})}{8\pi\hbar\varepsilon_0 cz_A^3}, \quad (108)$$

where the nonretarded limit of the Fresnel coefficients are given in Appendix B.

For the isotropic chiral medium we appreciate that the resulting frequency shifts are a superposition of the corresponding quantities of the perfectly conducting mirror of Sec. IV A and the perfectly reflecting chiral mirror of Sec. IV D determined by the Fresnel coefficients $r_{\sigma,\sigma'}$. As a result of that, all the previous discussions and mainly the conditions over \mathbf{v}_\parallel , \mathbf{d}_{nk} and \mathbf{e}_z discussed previously are valid here too. In Table I we resume the behavior that an isotropic chiral medium and its dipole moments \mathbf{d}_{nk} must have under P and T transformations, where both atom and medium exhibit true chirality. Moreover, the reflective coefficients are functions of the permittivity ε , the permeability μ and the chirality κ which could help to modulate the behavior of the spectroscopical quantities. In the same spirit as the role of the velocity's sign discussed for all the previous examples, the handedness of

the crossed Fresnel coefficients could increase or decrease the corresponding contribution just as found for the chiral mirror but now they are more complicated functions. Furthermore, in the nonretarded limit the contribution of the imaginary part of the crossed Fresnel coefficients in Eq. (108) becomes relevant because they could be more significant than the perfectly conductor behavior. Again, due to the internal connection between the frequency shift and the Casimir–Polder force, one can also switch from an attractive to a repulsive force between atom and medium.

V. DISCUSSION

As a first step towards observing motion–induced chirality and quantum friction with Rydberg atoms, we will discuss the magnitude of some key observables introduced above.

The central indicator of motion–induced chirality of the associated rotatory strength (91). Table II shows its magnitude for hydrogen in Rydberg states with a range of principal quantum numbers \bar{n} for the $|n\bar{0}0\rangle$ to $|n\bar{1}1\rangle$ transition and a velocity parallel to the plate of $v_{\parallel} = 300$ m/s.

It is interesting to compare this motion–induced rotatory strength with typical rotatory strengths of chiral molecules: For the S_0 – S_1 transition in the chiral carbonyl compounds fenchone and camphor, for instance, the rotatory strength corresponds to about 9.5×10^{-55} C²m³/s and 1.5×10^{-54} C²m³/s, respectively [91, 92]. Helicenes and their derivatives are known for comparatively large rotatory strengths, which range, depending on the specific transition selected, between around 1×10^{-56} C²m³/s and 1×10^{-53} C²m³/s for [4]-helicene, [5]-helicene and [6]-helicene [93–95]. The accompanying large isotropic optical dispersion of helicene derivatives qualifies them for instance as candidates for sensitive matterwave interference studies on chiral molecules as proposed in Ref. [96]. For the Rydberg atoms, we find that the associated rotatory strength is very high compared with regular rotatory strengths in chiral molecules, as it scales with the fourth-power of the principal quantum number. However, this scaling is rooted in the typical quadratic scaling of electrical dipoles in Rydberg systems, and thus, in relation to the electrical properties, the associated rotatory strength is still suppressed by a factor of v/c of the order of 10^{-6} .

To estimate the magnitude of motion-induced frequency shifts as evidence for quantum friction, we consider the bare and motion-corrected frequency shifts, Eqs. (62) and (63), respectively, of an atom at non-retarded distances $z_A = 1$ μ m from the surface of a perfectly reflecting nonreciprocal mirror. The results for a velocity $v = 300$ m/s are also displayed in Table II. Note that in (63) we need to choose the quantization axis in the \vec{v}_{\parallel} -direction parallel to the plate, which results in vanishing (62). In Table II we evaluate (62) there-

fore with respect to a quantization axis normal to the plate to allow for a useful comparison of the different frequency shifts. Additionally, Table II also gives values for frequency shifts in the analogue case of a chiral mirror (90), with adjusted transition states and quantization axis. Recent progress in the measurement of the transition frequency of Rydberg states has shown an accuracy of a few MHz using electromagnetically induced transparency [68] thus static dipole related energy shifts are resolvable starting from $n \geq 60$. Motion-corrected frequency shifts for a nonreciprocal mirror and a chiral mirror should be observable starting from $n \geq 40$ as kHz accuracy with Rydberg microwave Ramsey spectroscopy can be achieved when resorting to circular states [67]. Frequency shifts are advantageous for measurement because frequencies can be measured with very high accuracy [97]. In principle, laser excitation of Rydberg states is frequency selective to the width of the corresponding transition, where sub-kHz resolution in Rydberg states can be achieved for sufficiently high n . In the current application, state selective laser excitation might not be possible because of the proximity of the chiral mirror. Frequency measurement during free evolution of an atom excited to a Rydberg can be done via Ramsey interferometry. Interaction induced energy shifts lead to accumulated phase shifts, which can be projected to populations in a coherent excitation process, using other Rydberg states or a highly stable ground state as a reference. Measurements of interaction induced frequency shifts in Rydberg atoms have been measured [98] and proposed to be used in the application of chiral discrimination [54].

VI. CONCLUSIONS

In this work macroscopic QED was used to derive expressions for the Casimir–Polder frequency shift and spontaneous decay rate for a moving atom parallel to nonreciprocal (falsely chiral) and (truly) chiral media. The former violate Lorentz’s reciprocity principle meaning that time-reversal-symmetry is broken and the latter are reciprocal media breaking parity. Nonreciprocal media are included by using generalised real and imaginary parts of the Green’s tensor which reduce to the standard definitions in the reciprocal case, including (truly) chiral media.

The basis of our study lies on the interaction Hamiltonian between the atom, the field and the nonreciprocal or chiral medium, which enables us to obtain an expression for the electric and magnetic field. To this end, noise currents were quantized directly yielding one set of field operators for the combined electric and magnetic field. The result for both fields allowed us to analyze the internal atomic dynamics. Through the redefinitions of the real and imaginary parts of a tensor, we provide general expressions for the atomic decay rate and the frequency shift, which can be split into two kinds of terms. One depends only on the position and another one depends on

$\bar{n} =$	20	40	60	80
R_{nk}	1.291×10^{-51}	2.069×10^{-50}	1.048×10^{-49}	3.312×10^{-49}
$\delta\omega_{nk}$	2.918×10^7	4.677×10^8	2.369×10^9	7.487×10^9
$\delta\omega_{nk}(v)$ (nonreciprocal)	9.173×10^1	1.470×10^3	7.446×10^3	2.354×10^4
$\delta\omega_{nk}(v)$ (chiral)	1.835×10^2	2.941×10^3	1.489×10^4	4.707×10^4

TABLE II: Associated rotatory strength R_{nk} (91), bare and motion-corrected frequency shifts (62) and (63) for a nonreciprocal mirror, as well as motion-induced frequency shift (90) for a chiral mirror. The non-reciprocal frequency shift is given for an electrical dipole transition via Rydberg type states $\mathbf{d}_{nk} = \langle \bar{n}_n l_n m_n | \hat{\mathbf{d}} | \bar{n}_k l_k m_k \rangle = \langle \bar{n} 11 | \hat{\mathbf{d}} | \bar{n} 00 \rangle$, where the bare value is quantized in the z -direction, while for the motion induced shift the quantization axis is chosen parallel to \mathbf{v}_{\parallel} . The chiral frequency shift is calculated for an electrical dipole transition via Rydberg type states $\mathbf{d}_{nk} = \langle \bar{n}_n l_n m_n | \hat{\mathbf{d}} | \bar{n}_k l_k m_k \rangle = \langle \bar{n} 10 | \hat{\mathbf{d}} | \bar{n} 00 \rangle$, with quantization axis along $\mathbf{e}_y + \mathbf{e}_z$ for $\mathbf{v}_{\parallel} = v_{\parallel} \mathbf{e}_x$. All values are in standard SI-units, $[R] = \text{C}^2 \text{m}^3 / \text{s}$, $[\delta\omega] = \text{rad/s}$. Note that the velocity dependent values are linear in $v = |\mathbf{v}_{\parallel}|$ and the frequency shifts scale with z_A^{-3} ; the given values are calculated for the velocity $|\mathbf{v}_{\parallel}| = 300 \text{m/s}$ and at a distance $z_A = 10^{-6} \text{m}$.

the position and the velocity of the atom. Also we found that such terms can be split into resonant and nonresonant contributions. These results reproduce and extend the previous results for the static case of Ref. [64] for a polarizable atom moving parallel to nonreciprocal or chiral media.

By regarding only a moving non-magnetic atom we analyzed five different materials: a perfectly conducting mirror, a perfectly reflecting nonreciprocal mirror, a three-dimensional topological insulator, a perfectly reflecting chiral mirror and an isotropic chiral medium. We find different power laws for all these materials in the nonretarded limit and oscillating functions whose amplitudes decay with the distance in the retarded one.

Let us begin by summarising the results for the static frequency shift of the nonreciprocal media. By employing an arbitrary dipole moment, we are able to generalize the results of Ref. [64]. Finding that for the perfectly conducting mirror there is no difference between any special polarizations because its frequency shift depends only on the magnitude of the dipole moments, i.e. all of them will always contribute. More interesting are the results for the nonreciprocal mirror, because its frequency shift depends on $\text{Im}(d_{nk}^x d_{nk}^{y*})$ which rewritten as Eq. (64) can be identified as the z component of the geometric magnetic field \mathcal{B}_z associated with photoionization of chiral molecules [72, 73]. This constitutes the first bridge between the physics of chirality and nonreciprocity obtained in this work: nonreciprocal media couple to the falsely chiral response of the molecule. For the strong 3D TI we found that its frequency shift is a superposition of the perfectly conducting mirror and the nonreciprocal mirror ones but modulated by the Fresnel coefficients. The latter provide the possibility to modulate the behavior of the spectroscopical quantities by adjusting the permittivity ε and mainly the topological parameter Δ because it can be negative for certain strong 3D TIs. All these results reproduce the same algebraic power laws and fading out functions found in Ref. [64] for the nonretarded and retarded limits respectively.

Now we move on with the results for the static frequency shift of the chiral media. For the perfectly reflecting chiral mirror and the isotropic chiral medium these

spectroscopical quantities are identically zero. According to Curie's principle [69] these results are reasonable because our chosen dipole moments do not share the same symmetry. The square of the transition dipoles constitute an achiral response that is unable to resolve the chirality is present in both materials. So, to probe the chirality one should employ a molecule with a magnetic moment as well as an electric one.

On the other hand, we have the velocity-dependent the frequency shift of the nonreciprocal media. After employing again an arbitrary dipole moment, we find that for the perfectly conducting mirror the relevant vectorial structure is $S_{nk}(\mathbf{v}_{\parallel}) = \text{Im}[(\mathbf{d}_{nk}^* \cdot \mathbf{e}_z)(\mathbf{d}_{nk} \cdot \mathbf{v}_{\parallel})]$, which is zero from Maxwell equations conditions leading to a vanishing shift and guarantees the P -even and T -even behavior of this material. For the nonreciprocal mirror the vectorial structure can be understood in terms of the nonreciprocal optical rotatory strength $T_{nk}(\mathbf{v}_{\parallel}) = \text{Re}\{(\mathbf{d}_{nk}^* \cdot \mathbf{e}_z)[(\mathbf{v}_{\parallel} \times \mathbf{d}_{nk}) \cdot \mathbf{e}_z]\}$ given by Eq. (68) which needs a superposition of linear polarized dipoles to not vanish. Because of its similarity with the optical rotatory strength of chiral media, this constitutes the second bridge found in this work between the physics of chirality and nonreciprocity. Then, we analyzed the frequency shift of a strong 3D TI. In this case, we found again that its frequency shift is a superposition of the perfectly conducting mirror and the nonreciprocal mirror ones but modulated by the Fresnel coefficients. However, the sign of the velocity could lead to an enhancement or decrease on the effect for the three materials, but for the strong 3D TI the topological parameter Δ is another quantity that has this feature. Algebraic power laws in the atom's distance z_A to the interface are provided for the three materials in the nonretarded limits, which could be useful for experimental verification. All these results are consistent with Curie's principle because T_{nk} is a T -odd quantity and also the strong 3D TI breaks time-reversal symmetry via the topological parameter Δ being a T -odd quantity. For this reason, this study gains significance for ongoing investigations into dark matter detection, where axions emerge as a promising candidate [99]. In this pursuit, condensed matter physics offers novel avenues through TIs [100], antiferromagnetically doped TIs

[101, 102], or multiferroics [103], utilizing the magneto-electric effect which underpins our results.

Regarding the velocity-dependent frequency shift of the chiral media. Let us describe first the results for the perfectly reflecting chiral mirror. Here we found that this spectroscopical quantity is determined by $R_{nk}(\mathbf{v}_{\parallel}) = \text{Im} \{ (\mathbf{d}_{nk}^* \cdot \mathbf{e}_z) [(\mathbf{v}_{\parallel} \times \mathbf{d}_{nk}) \cdot \mathbf{e}_z] \}$ which is the optical rotatory strength [59, 60] given by Eq. (91). Therefore, we can interpret that an effective circular dichroism of the transition $n \leftarrow k$ between the electric dipole \mathbf{d}_{nk} and the effective magnetic moment $\mathbf{m}_{nk} = -\mathbf{v}_{\parallel} \times \mathbf{d}_{nk}$. Although we did not employ a chiral source, the rectilinear uniform motion of our electric dipole induces an effective magnetic moment through its velocity as found in Eq. (67), therefore a chiral source is indirectly used to probe the chirality of this mirror explaining the non-zero results, i.e., here occurs a motion-induced (true) chirality. Lastly, for the isotropic chiral medium its frequency shift are a superposition of the perfectly conducting mirror and the chiral mirror ones but modulated by the Fresnel coefficients. For both chiral materials the sign of the velocity and the handedness of the media could lead to an enhancement or decrease on the effect. Algebraic power laws in the atom's distance z_A to the interface are provided for these two materials in the nonretarded limits, which could be useful for experimental verification. Nevertheless, for the isotropic chiral medium the complex character of the Fresnel coefficient can enhance the power law of the distance to the surface. All these results are consistent with Curie's principle because R_{nk} is a P -odd quantity, if circular or elliptical polarizations are selected, and also the isotropic chiral medium breaks the parity symmetry via its chirality κ being a P -odd quantity.

It is worth to mention a few comments before closing this section. First, for the current interface Δ is proportional to the fine structure α as mentioned in Eq. (76). Nevertheless, we could replace the strong 3D TI by a magnetoelectric such as TbPO_4 whose $\Delta = 0.22$ [82, 83] increases the influence of the non-reciprocal medium. But we focus on the current work only on strong 3D TIs. Second, the present work provides general results for the frequency shifts either resonant or nonresonant but we remark that all the concrete results for the five materials are valid only for real permittivities and non-magnetic strong 3D TIs, i.e. for the five materials their susceptibilities do not have frequency dependence. Third, due to a more exhaustive analysis of the frequency derivative involved in the velocity-dependent decay rates, we have left their study for these materials for future work. Fourth, of course the study of the perpendicular motion ($v_z \neq 0$) can be investigated but it has problems and we will leave it for further studies, which resembles the classical situation of transition radiation studied previously in Ref. [49]. Finally, all these results are obtained within the Markovian framework meaning that they are only valid for times that verify the constraints described in Ref. [32].

VII. ACKNOWLEDGMENTS

We would like to thank Stephen Barnett, Lawrence D. Barron, Robert Bennett, Quentin Bouton, Carsten Henkel, Francesco Intravaia, Athanasios Laliotis, Daniel Reiche and Fumika Suzuki for discussions. O. J. F. has been supported by the postdoctoral fellowships CONACYT-770691, CONACYT-800966 and by the German Research Foundation. The authors gratefully acknowledge funding by the Deutsche Forschungsgemeinschaft (DFG, German Research Foundation) – Project No. 328961117 – SFB 1319 ELCH.

Appendix A: Fresnel reflection coefficients for a vacuum-strong 3D TI interface

To the purpose of this article be self-contained in this appendix we provide the necessary details of the reflective coefficients in the retarded and nonretarded limits for nonreciprocal media.

The Fresnel coefficients for an interface constituted by a 3D topological insulator with $\mu_2 = 1$ and vacuum in the retarded limit ($\tilde{\omega}_{nk}z_A/c \gg 1$) whose main contribution comes from the region due to small k_{\parallel} are [64]:

$$r_{s,s}^{\text{ret}} = \frac{1 - \varepsilon - \Delta^2}{(1 + \sqrt{\varepsilon_2})^2 + \Delta^2}, \quad (\text{A1})$$

$$r_{p,s}^{\text{ret}} = \frac{-2\Delta}{(1 + \sqrt{\varepsilon_2})^2 + \Delta^2}, \quad (\text{A2})$$

$$r_{p,p}^{\text{ret}} = -r_{s,s}^{\text{ret}}, \quad (\text{A3})$$

$$r_{s,p}^{\text{ret}} = r_{p,s}^{\text{ret}}, \quad (\text{A4})$$

where Δ is given by Eq. (76).

On the other hand, these coefficients in the nonretarded limit ($\tilde{\omega}_{nk}z_A/c \ll 1$) whose leading contribution comes from the region due to large k_{\parallel} are [64]:

$$r_{s,s}^{\text{nret}} = \frac{-\Delta^2}{2(\varepsilon_2 + 1) + \Delta^2}, \quad (\text{A5})$$

$$r_{s,p}^{\text{nret}} = \frac{-2\Delta}{2(\varepsilon_2 + 1) + \Delta^2}, \quad (\text{A6})$$

$$r_{p,p}^{\text{nret}} = \frac{2(\varepsilon_2 - 1) + \Delta^2}{2(\varepsilon_2 + 1) + \Delta^2}, \quad (\text{A7})$$

$$r_{s,p}^{\text{nret}} = r_{p,s}^{\text{nret}}. \quad (\text{A8})$$

Appendix B: Fresnel reflection coefficients for the vacuum-isotropic chiral medium interface

The corresponding Fresnel coefficients for an interface constituted by an isotropic chiral medium and vacuum in the retarded limit ($\tilde{\omega}_{nk}z_A/c \gg 1$) whose main contri-

bution comes from the region due to small k_{\parallel} are [104]:

$$\begin{aligned} r_{s,p}^{\text{ret}} &= \frac{2i(k_L|k_R| - k_R|k_L|)}{2\left(\frac{\varepsilon+\mu}{n_r}\right)(k_L k_R + |k_R k_L|) + (k_L|k_R| + k_R|k_L|)}, \\ r_{p,s}^{\text{ret}} &= -r_{s,p}^{\text{ret}}, \\ r_{s,s}^{\text{ret}} &= \frac{2(k_L k_R - |k_R k_L|) - \left(\frac{\varepsilon-\mu}{n_r}\right)(k_L|k_R| + k_R|k_L|)}{2(k_L k_R + |k_R k_L|) + \left(\frac{\varepsilon+\mu}{n_r}\right)(k_L|k_R| + k_R|k_L|)}, \\ r_{p,p}^{\text{ret}} &= \frac{2(k_L k_R - |k_R k_L|) + \left(\frac{\varepsilon-\mu}{n_r}\right)(k_L|k_R| + k_R|k_L|)}{2(k_L k_R + |k_R k_L|) + \left(\frac{\varepsilon+\mu}{n_r}\right)(k_L|k_R| + k_R|k_L|)}, \end{aligned} \quad (\text{B1})$$

where we recall the definitions for k_R and k_L given in Eqs. (99) and (100). To obtain these coefficients, the

approximations $k^{\parallel} = 0$ and

$$k^{\perp} \simeq n_r \omega / c = \sqrt{\varepsilon(\omega)\mu(\omega)}\omega / c \quad (\text{B2})$$

were applied to their general expressions given in Ref. [84].

On the other hand, these coefficients in the nonretarded limit ($\tilde{\omega}_{nk} z_A / c \ll 1$) whose leading contribution comes from the region due to large k_{\parallel} are [60]:

$$r_{s,s}^{\text{nret}} = \frac{\varepsilon_2 \mu_2 - \kappa_2^2 - \varepsilon_2 + \mu_2 - 1}{\varepsilon_2 \mu_2 - \kappa_2^2 + \varepsilon_2 + \mu_2 + 1}, \quad (\text{B3})$$

$$r_{p,s}^{\text{nret}} = \frac{-2i\kappa_2}{\varepsilon_2 \mu_2 - \kappa_2^2 + \varepsilon_2 + \mu_2 + 1}, \quad (\text{B4})$$

$$r_{p,p}^{\text{nret}} = \frac{\varepsilon_2 \mu_2 - \kappa_2^2 + \varepsilon_2 - \mu_2 - 1}{\varepsilon_2 \mu_2 - \kappa_2^2 + \varepsilon_2 + \mu_2 + 1}, \quad (\text{B5})$$

$$r_{s,p}^{\text{nret}} = -r_{p,s}^{\text{nret}}. \quad (\text{B6})$$

-
- [1] H. B. Casimir, Proc. K. Ned. Akad. Wet. **51**, 793 (1948).
[2] P. W. Milonni, *The Quantum Vacuum: An Introduction to Quantum Electrodynamics* (Academic; New York, 2013).
[3] D. A. R. Dalvit, P. W. Milonni, D. Roberts and F. S. S. Rosa, *Casimir Physics*, Lecture Notes in Physics (Springer-Verlag, Heidelberg, 2011).
[4] L. M. Woods, D. A. R. Dalvit, A. Tkatchenko, P. Rodriguez-Lopez, A. W. Rodriguez and R. Podgornik, Rev. Mod. Phys. **88**, 045003 (2016).
[5] H. B. G. Casimir and D. Polder, Phys. Rev. **73**, 360 (1948).
[6] J. B. Pendry, J. Phys: Condens. Matter **9**, 10301 (1997).
[7] A. I. Volokitin and B. N. J. Persson, Rev. Mod. Phys. **79**, 1291 (2007).
[8] J. B. Pendry, New J. Phys. **12**, 033028 (2010).
[9] Mario G Silverinha, New J. Phys. **16**, 063011 (2014).
[10] M. Belen Farias, Wilton J. M. Kort-Kamp and Diego A. R. Dalvit, Phys. Rev. B **97**, 161407(R) (2018).
[11] S. Scheel and S. Y. Buhmann, Phys. Rev. A **80**, 042902 (2009).
[12] F. Intravaia, R. O. Behunin and D. A. R. Dalvit, Phys. Rev. A **89**, 050101.
[13] F. Intravaia, R. O. Behunin, C. Henkel, K. Busch and D. A. R. Dalvit, Phys. Rev. Lett. **117**, 100402 (2016).
[14] R. Zhao, A. Manjavacas, F. J. Garcia de Abajo and J. B. Pendry, Phys. Rev. Lett. **109**, 123604 (2012).
[15] A. I. Volotkin, JETP Letters **104**, 504-509 (2016); M. B. Farias, C. D. Fosco, F. C. Lombardo and F. D. Mazzitelli, Phys. Rev. D **95**, 065012 (2017).
[16] V. Frolov and V. Ginzburg. Phys. Lett. A **116**, 423 (1986).
[17] M. V. Nezlin, Sov. Phys. Usp. **19**, 946, (1976).
[18] V. L. Ginzburg, Phys. Usp. **39**, 973 (1996).
[19] M. F. Maghrebi, R. Golestanian and M. Kardar, Phys. Rev. A **88**, 042509 (2013).
[20] F. Intravaia, V. E. Mkrtchian, S. Y. Buhmann, S. Scheel, D. A. R. Dalvit and C. Henkel, J. Phys. Condens. Matter **27**, 214020 (2015).
[21] G. Dedkov and A. Kyasov, Phys. Solid State **44**, 1809 (2002).
[22] G. Barton, New J. Phys. **12**, 113045 (2010).
[23] M. G. Silverinha and S. I. Maslovski, Phys. Rev. A **86**, 042118 (2012); G. Pieplow and C. Henkel, New J. Phys. **15**, 023027 (2013); U. D. Jentschura, G. Lach, M. De Kieviet and K. Pachucki, Phys. Rev. Lett. **114**, 043001 (2015); A. I. Volotkin, Phys. Rev. A **96**, 012520 (2017); F. C. Lombardo and P. I. Villar, J. Phys. Conf. Ser. **880**, 012035 (2017); P. Rodriguez-Lopez and E. Martın-Martınez, Phys. Rev. A **98**, 032507 (2018).
[24] J. Klatt, R. Bennett and S. Y. Buhmann, Phys. Rev. A **94**, 063803 (2016).
[25] F. Intravaia, R. O. Behunin, C. Henkel, K. Busch and D. A. R. Dalvit, Phys. Rev. A **94**, 042114 (2016).
[26] F. Intravaia, M. Oelschlager, D. Reiche, D. A. R. Dalvit and K. Busch, Phys. Rev. Lett. **123**, 120401 (2019).
[27] M. B. Pogrebinskii, Fiz. Tekh. Poluprovodn. (S.-Peterburg) **11**, 637 (1977) [Sov. Phys. Semicond. **11**, 372 (1977)]; P. J. Price, Physica **117B-118B**, 750 (1983); A. I. Volokitin and B. N. J. Persson, Phys. Rev. Lett. **106**, 094502 (2011).
[28] T. J. Gramila, J. P. Eisenstein, A. H. MacDonald, L. N. Pfeiffer and K. W. West, Phys. Rev. Lett. **66**, 1216 (1991); R. V. Gorbachev, A. K. Geim, M. I. Katsnelson, K. S. Novoselov, T. Tudorovskiy, T. V. Grigorieva, A. H. MacDonald, K. Watanabe, T. Taniguchi and L. P. Ponomarenko, Nat. Phys. **8**, 896 (2012).
[29] S. Y. Buhmann. *Dispersion Forces I. Macroscopic Quantum Electrodynamics and Ground-State Casimir, Casimir-Polder and van der Waals Forces* (Springer, Berlin Heidelberg, 2012).
[30] See, for example: S. Y. Buhmann, L. Knoll, D.-G. Welsch, and H. T. Dung. Phys. Rev. A **70**, 052117 (2004); S. Scheel and S. Y. Buhmann, Acta Physica

- Slovaca **58**, 675 (2008).
- [31] S. Y. Buhmann *Dispersion Forces II. Many-Body Effects, Excited Atoms, Finite Temperature and Quantum Friction* (Springer, Berlin Heidelberg, 2012).
- [32] Juliane Klatt, Chahan M. Kropf and Stefan Y. Buhmann. Phys. Rev. Lett. **126**, 210401 (2021).
- [33] Nikita Kavokine, Marie-Laure Bocquet and Lydéric Bocquet. Nature **602**, 84 (2022).
- [34] M. Z. Hasan and C. L. Kane, Rev. Mod. Phys. **82**, 3045 (2010).
- [35] X. L. Qi and S. C. Zhang, Rev. Mod. Phys. **83**, 1057 (2011).
- [36] L. Fu, C. L. Kane and E. J. Mele, Phys. Rev. Lett. **98**, 106803 (2007); L. Fu and C. L. Kane, Phys. Rev. B **76**, 045302 (2007).
- [37] J. E. Moore and L. Balents, Phys. Rev. B **75**, 121306(R) (2007); R. Roy, Phys. Rev. B **79**, 195322 (2009).
- [38] M. Morgenstern, C. Pauly, J. Kellner, M. Liebmann, M. Pratzner, G. Bihlmayer, M. Eschbach, L. Plucinski, S. Otto, B. Rasche, M. Ruck, M. Richter, S. Just, F. Lüpkke, and B. Voigtländer, Phys. Status Solidi B **258**, 2000060 (2021).
- [39] D. Hsieh, D. Qian, L. Wray, Y. Xia, Y. S. Hor, R. J. Cava, and M. Z. Hasan, Nature (London) **452**, 970 (2008).
- [40] Y. Xia, D. Qian, D. Hsieh, L. Wray, A. Pal, H. Lin, A. Bansil, D. Grauer, Y. S. Hor, R. J. Cava and M. Z. Hasan, Nat. Phys. **5**, 398 (2009); H. Zhang, C.-X. Liu, X.-L. Qi, X. Dai, Z. Fang, and S.-C. Zhang, Nat. Phys. **5**, 438 (2009); Y. Ando, J. Phys. Soc. Japan **82**, 102001 (2013).
- [41] D. Xiao, J. Jiang, J.-H. Shin, W. Wang, F. Wang, Y.-F. Zhao, C. Liu, W. Wu, M. H.-W. Chan, N. Samarth and C.-Z. Chang, Phys. Rev. Lett. **120**, 056801 (2018); M. Mogi, M. Kawamura, A. Tsukazaki, R. Yoshimi, K. S. Takahashi, M. Kawasaki and Y. Tokura, Sci. Adv. **3**, 1669 (2017); Nicodemos Varnava and David Vanderbilt, Phys. Rev. B **98**, 245117 (2018).
- [42] C.-Z. Chang, J. Zhang, X. Feng, J. Shen, Z. Zhang, M. Guo, K. Li, Y. Ou, P. Wei, L.-L. Wang, Z.-Q. Ji, Y. Feng, S. Ji, X. Chen, J. Jia, X. Dai, Z. Fang, S.-C. Zhang, K. He, Y. Wang et al., Science **340**, 167 (2013); X. K. Kou, S.-T. Guo, Y. Fan, L. Pan, M. Lang, Y. Jiang, Q. Shao, T. Nie, K. Murata, J. Tang, Y. Wang, L. He, T.-K. Lee, W.-L. Lee and K. Wang, Phys. Rev. Lett. **113**, 137201 (2014); J. G. Checkelsky, R. Yoshimi, A. Tsukazaki, K. S. Takahashi, Y. Kozuka, J. Falson, M. Kawasaki and Y. Tokura, Nat. Phys. **10**, 731 (2014); C. Z. Chang, W. Zhao, D. Y. Kim, H. Zhang, B. A. Assaf, D. Heiman, S.-C. Zhang, C. Liu, M. H. W. Chan and J. S. Moodera, Nat. Mater. **14**, 473 (2015).
- [43] M. Mogi, M. Kawamura, R. Yoshimi, A. Tsukazaki, Y. Kozuka, N. Shirakawa, K. S. Takahashi, M. Kawasaki and Y. Tokura, Nat. Mater. **16**, 516-521 (2017).
- [44] L. Wu, M. Salehi, N. Koirala, J. Moon, S. Oh and N. P. Armitage, Science **354**, 1124-1127 (2016).
- [45] V. Dziom, A. Shuvaev, A. Pimenov, G. V. Astakhov, C. Ames, K. Bendias, J. Böttcher, G. Tkachov, E. M. Hankiewicz, C. Brüne, H. Buhmann and L. W. Molenkamp, Nat. Commun. **8**, 15197 (2017).
- [46] X. L. Qi, T. L. Hughes, S. C. Zhang, Phys. Rev. B **78**, 195424 (2008).
- [47] K. N. Okada, Y. Takahashi, M. Mogi, R. Yoshimi, A. Tsukazaki, K. S. Takahashi, N. Ogawa, M. Kawasaki and Y. Tokura, Nat. Commun. **7**, 12245 (2016).
- [48] O. J. Franca, L. F. Urrutia and Omar Rodríguez-Tzompantzi. Phys. Rev. D **99**, 116020 (2019).
- [49] O. J. Franca and Stefan Yoshi Buhmann, Phys. Rev. B **105**, 155120 (2022).
- [50] O. J. Franca and L. F. Urrutia. Revista Mexicana de Física **68**, 060701 (2022).
- [51] O. J. Franca and Stefan Yoshi Buhmann, Phys. Rev. B **110**, 195150 (2024).
- [52] X. L. Qi, R. D. Li, J. D. Zang, and S. C. Zhang, Science **323**, 1184 (2009).
- [53] Jorge David Castaño-Yepes, O. J. Franca, C.F. Ramirez-Gutierrez and J.C. del Valle. Physica E **123**, 114202 (2020).
- [54] S. Y. Buhmann, S. M. Giesen, M. Diekmann, R. Berger, S. Aull, P. Zahariev, M. Debatin and K. Singer. New J. Phys. **23**, 083040 (2021).
- [55] E. U. Condon. Rev. Mod. Phys. **9**, 432 (1937).
- [56] P. Král, I. Thanopoulos, M. Shapiro and D. Cohen. Phys. Rev. Lett. **90** 033001 (2003).
- [57] D. Vardanega, F. Picaud and C. Giradet. Surf. Sci. **601**, 3818 (2007).
- [58] J. Trost and K. Hornberger. Phys. Rev. Lett. **103**, 023202 (2009).
- [59] D. Craig D P and T. Thirunamachandran. *Molecular Quantum Electrodynamics* (New York: Academic, 1984).
- [60] David T. Butcher, Stefan Yoshi Buhmann and Stefan Scheel. New J. Phys. **14**, 113013 (2012).
- [61] Pablo Barcellona, Hassan Safari, A. Salam and Stefan Yoshi Buhmann. Phys. Rev. Lett. **118**, 193401 (2017).
- [62] Fumika Suzuki, Takamasa Momose and Stefan Yoshi Buhmann. Phys. Rev. A **99**, 012513 (2019).
- [63] Stefan Yoshi Buhmann, David T Butcher and Stefan Scheel. New Journal of Physics **14** (2012) 083034.
- [64] S. Fuchs, J. A. Crosse, S. Y. Buhmann, Phys. Rev. A **95**, 023805 (2017).
- [65] L. Onsager, Phys. Rev. **37**, 405 (1931).
- [66] H. A. Lorentz, Koninklijke Nederlandse Akademie van Wetenschappen te Amsterdam **4**, 176 (1896).
- [67] J. Zou and S. D. Hogan, Phys. Rev. A **107**, 062820 (2023).
- [68] B. S. Silpa, K. B. Shovan, C. Saptarishi, and R. Sanjukta, Opt. Continuum **1**, 1176192 (2022)
- [69] P. Curie, J. Phys. Theor. Appk. **3**, 393 (1894).
- [70] J. A. Crosse, S. Fuchs, S. Y. Buhmann, Phys. Rev. A **92**, 063831 (2015).
- [71] Stefan Yoshi Buhmann, Valery N. Marachevsky and Stefan Scheel, Phys. Rev. A **98**, 022510 (2018).
- [72] David Ayuso, Andres F. Ordonez and Olga Smirnova. Phys. Chem. Chem. Phys. **24**, 26962 (2022)
- [73] A. F. Ordonez and O. Smirnova. Phys. Rev. A **99**, 043416 (2019).
- [74] Stefan Scheel and Stefan Yoshi Buhmann, Acta Phys. Slovaca **58**, 675 (2008).
- [75] R. Noguchi, T. Takahashi, K. Kuroda, M. Ochi, T. Shirasawa, M. Sakano, C. Bareille, M. Nakayama, M. D. Watson, K. Yaji, A. Harasawa, H. Iwasawa, P. Dudin, T. K. Kim, M. Hoesch, V. Kandyba, A. Giampietri, A. Barinov, S. Shin, R. Arita et al., Nature **566**, 518 (2019).
- [76] Inbar Hotzen Grinberg, Mao Lin, Wladimir A. Benalcazar, Taylor L. Hughes, and Gaurav Bahl, Phys. Rev. Applied **14**, 064042 (2020).

- [77] A. Martín-Ruiz, M. Cambiaso and L. F. Urrutia, *Phys. Rev. D* **92**, 125015 (2015).
- [78] A. Martín-Ruiz, M. Cambiaso and L. F. Urrutia. *EPL* **113**, 60005 (2016).
- [79] T. H. O'Dell, *The Electrodynamics of Magneto-Electric Media* (North-Holland, Amsterdam, 1970).
- [80] L. D. Landau, E. M. Lifshitz and L. P. Pitaevskii. *Electrodynamics of Continuous Media, Course of Theoretical Physics Vol. 8* (Pergamon Press, Oxford, 1984).
- [81] F.W. Hehl, Y.N. Obukhov, J.-P. Rivera and H. Schmid, Relativistic analysis of magnetoelectric crystals: Extracting a new 4-dimensional P odd and T odd pseudoscalar from Cr_2O_3 data, *Phys. Lett. A* **372**, 1141-1146 (2008).
- [82] S. S. Batsanov, E. D. Ruchkin, I. A. Poroshina, *Refractive Indices of Solids* (SpringerBriefs in Applied Sciences and Technology, Singapore, 2016).
- [83] J. -P. Rivera, *Eur. Phys. J. B* **71**, 299 (2009).
- [84] S. M. Ali, T. M. Habashy and J. A. Kong. *J. Opt. Soc. Am. A* **9**, 413 (1992).
- [85] Christophe Caloz and Ari Sihvola. arXiv: 1903.09087 [physics.optics]
- [86] A. Lakhtakia, V. K. Varadan, V.V. Varadan, *Time-Harmonic Electromagnetic Fields in Chiral Media*, Springer-Verlag 1989.
- [87] I. V. Lindell, A. H. Sihvola, S. A. Tretyakov, and A. J. Viitanen, *Electromagnetic Waves in Chiral and Bi-isotropic Media*, (Artech House Publishers, 1994).
- [88] L. D. Barron, *Chemical Physics Letters* **123**, 423 (1986).
- [89] L. D. Barron, *J. Am. Chem. Soc.* **108**, 5539 (1986).
- [90] L. D. Barron, private communication (2024).
- [91] L. A. Kerber, O. Kreuz, T. Ring, H. Braun, R. Berger, and D. M. Reich, arXiv:2405.12893, (2024).
- [92] F. Pulm, J. Schramm, J. Hormes, S. Grimme, and S. D. Peyerimhoff, *Chem. Phys.* **224**, 143 (1997).
- [93] A. Brown, C. Kemp, and S. Mason, *Mol. Phys.* **20**, 787 (1971)
- [94] A. Brown, C. M. Kemp, and S. F. Mason, *J. Chem. Soc. A*, 751 (1971)
- [95] W. S. Brickell, A. Brown, C. M. Kemp, and S. F. Mason, *J. Chem. Soc. A*, 756 (1971).
- [96] B. A. Stickler, M. Diekmann, R. Berger, D. Wang, *Phys. Rev. X* **11**, 031056 (2021).
- [97] Keller, J., Burgermeister, T., Kalincev, D., Kiethe, J. and Mehlstäubler, T. *Journal Of Physics: Conference Series* **723**, 012027 (2016).
- [98] Arias, A., Lochead, G., Wintermantel, T., Helmrich, S. and Whitlock, S. *Phys. Rev. Lett.* **122**, 053601 (2019).
- [99] P. Sikivie, *Rev. Mod. Phys.* **93**, 15004 (2021).
- [100] Dennis M. Nenno, Christina A. C. Garcia, Johannes Gooth, Claudia Felser and Prineha Narang, *Nat. Rev. Phys.* **2**, 682 (2020).
- [101] David J.E. Marsh, Kin Chung Fong, Erik W. Lentz, Libor Šmejkal and Mazhar N. Ali, *Phys. Rev. Lett.* **123**, 121601 (2019).
- [102] Jan Schütte-Engel, David J.E. Marsh, Alexander J. Millar, Akihiko Sekine, Francesca Chadha-Day, Sebastian Hoof, Mazhar N. Ali, Kin Chung Fong, Edward Hardy and Libor Šmejkal, *JCAP* **08**, 066 (2021).
- [103] Henrik S. Røising, Benjo Fraser, Sinéad M. Griffin, Sumanta Bandyopadhyay, Aditi Mahabir, Sang-Wook Cheong and Alexander V. Balatsky, *Phys. Rev. Research* **3**, 033236 (2021).
- [104] C. S. Rapp, Janine C. Franz, Stefan Yoshi Buhmann and O. J. Franca, arXiv:2406.10038 [quant-ph]